THE ASTROPHYSICAL JOURNAL SUPPLEMENT SERIES, 118:327–352, 1998 October

THE MOLONGLO REFERENCE CATALOG 1 Jy RADIO SOURCE SURVEY. III. IDENTIFICATION OF A COMPLETE QUASAR SAMPLE

VIJAY K. KAPAHI, RAMANA M. ATHREYA, AND C. R. SUBRAHMANYA
National Centre for Radio Astrophysics, TIFR, Pune University Campus, Ganeshkhind, Pune-411007, India; vijay@ncra.tifr.res.in, ramana@ncra.tifr.res.in, crs@ncra.tifr.res.in

JOANNE C. BAKER[1]
School of Physics, University of Sydney, NSW 2006, Australia; jcb@mrao.cam.ac.uk

RICHARD W. HUNSTEAD
School of Physics, University of Sydney, NSW 2006, Australia; RWH@astrop.physics.usyd.edu.au

PATRICK J. MCCARTHY
The Observatories of the Carnegie Institution of Washington, 813 Santa Barbara Street, Pasadena, CA 91101; pmc2@ocwi.edu

AND

WIL VAN BREUGEL
Institute for Geophysics and Planetary Physics, LLNL, P.O. Box 808, L-413, Livermore, CA 94551; wil@sunlight.llnl.gov
Received 1998 February 5; accepted 1998 May 1

ABSTRACT

We present a new complete sample of 111 radio quasars (including six BL Lac objects) selected from the Molonglo Reference Catalog (MRC) at 408 MHz. The sample, which we call the Molonglo Quasar Sample (MQS), forms part of a complete survey of 557 MRC radio sources with $S_{408} \geq 0.95$ Jy in the declination range $-30° < \delta < -20°$, $b > 20°$ but excluding the R.A. range $14^{\rm h}03^{\rm m}$–$20^{\rm h}20^{\rm m}$. Quasar classifications are based on high-resolution radio images, deep optical identifications, and follow-up spectroscopy of sources in the strip. The relatively low radio frequency of the finding survey and the complete optical identification of quasars to faint magnitudes ensure that the MQS is relatively free from orientation biases that affect most other samples of radio-loud quasars. The MQS is therefore particularly well suited to investigating the effects of radio axis orientation on quasar properties. This paper describes in detail the formation of the MQS and presents basic radio and optical data, including VLA images of extended radio sources in the sample and a complete set of optical finding charts.

Subject headings: galaxies: structure — quasars: general — radio continuum: galaxies — surveys

1. INTRODUCTION

It has become increasingly clear in recent years that orientation-dependent effects play an important role in the classification of different types of active galactic nuclei (AGNs). This concept has spawned several "unified schemes," which seek to explain the observed differences between many subclasses of AGNs in terms of different viewing directions to intrinsically similar objects (see review by Antonucci 1993). One of the first and arguably most successful such proposals was the unification of lobe-dominated steep-spectrum radio quasars and core-dominated flat-spectrum quasars based on relativistic beaming effects in their nuclear jets (Kapahi & Saikia 1982; Orr & Browne 1982). In this scheme, Doppler boosting, associated with relativistic bulk motion of material in the approaching nuclear jet, occurs in sources viewed with their jet axis close to the line of sight, which results in the core flux density appearing to dominate over that of the extended lobes (which are presumed to be moving at sub-relativistic speeds). The strong Doppler boosting in the cores, together with their flatter radio spectra compared with the extended lobes, implies that flux-limited surveys at higher radio frequencies will preferentially select a larger fraction of core-dominated objects (Orr & Browne 1982), as is observed to be the case. Consequently, quasars found in gigahertz surveys will clearly not have their jet axes oriented randomly on the sky. On the other hand, quasar samples formed from surveys at low radio frequencies, where cores generally make an insignificant contribution to the total flux density, will be much less strongly biased in the orientation of their jet axes.

Most quasar samples are also limited in optical apparent magnitude. With the sole exception, perhaps, of quasars drawn from the completely identified and relatively bright 3CRR catalog (Laing, Riley, & Longair 1983), samples of radio-loud quasars available in the literature are all subject to an optical as well as a radio flux density limit. This is because the optical identification of radio sources with stellar objects—the first step in forming samples of radio quasars—has generally been based on positional agreement using magnitude-limited sky survey material. However, there is now considerable evidence that the optical continuum radiation of quasars is also anisotropic (Browne & Wright 1985; Jackson & Browne 1989; Baker 1997). Any optical magnitude limit can therefore result in intrinsically less luminous quasars being preferentially selected because of their favorable orientations (Kapahi & Shastri 1987). This implies that selection at low radio frequencies is not sufficient by itself to ensure a reasonably random distribution of orientations; it is also necessary that identifications be based on deep optical images to ensure that no sources remain unidentified. The existing quasar samples selected from low-frequency catalogs, such as the 4C survey at 178 MHz (e.g., Wills & Lynds 1978; Wills 1979; Stannard &

[1] MRAO, Cavendish Laboratory, Madingley Road, Cambridge CB3 0HE, UK.

Neal 1977; Hooley, Longair, & Riley 1978) and the B2 (Fanti et al. 1977) and B3 (Vigotti et al. 1997) surveys at 408 MHz all suffer from such biases.

In order to minimize these biases and to investigate how orientation affects other quasar properties, we have defined a new complete sample of radio quasars selected from the 408 MHz Molonglo Reference Catalog (MRC: Large et al. 1981). This sample, which we call the Molonglo Quasar Sample (MQS), contains all MRC quasars with $S_{408} > 0.95$ Jy in a 10° strip of the southern sky, $-30° < \delta < -20°$, and Galactic latitude $b > 20°$ but excluding the R.A. range of $14^{\rm h}03^{\rm m}$–$20^{\rm h}20^{\rm m}$. The identification of the MQS has been undertaken largely in parallel with that of the complementary survey comprising all MRC sources with $S_{408} > 0.95$ Jy in the same strip of sky (mostly radio galaxies). The final quasar classifications are based on considerable observational data, including high-resolution radio images, deep optical identifications, and detailed spectroscopic observations. With the parent survey, the MQS forms part of a major project to study the radio and optical properties of a complete sample of radio sources at intermediate flux densities (McCarthy et al. 1996, hereafter Paper I).

In this paper we describe first how the MQS was formed, in rough chronological order, and then present basic radio and optical data for the final sample of 111 objects (including six BL Lac objects). VLA radio images and a complete set of optical finding charts are also presented here. Optical spectroscopy of 80 Molonglo quasars will be published in a subsequent paper (Baker et al. 1998, hereafter Paper IV). Radio galaxy identifications from the MRC survey are given in Paper I, with follow-up radio data in Paper II (Kapahi et al. 1998). Some results based on analysis of the radio and optical properties of the MQS in an earlier (though somewhat incomplete) listing of the sample have already been reported (Kapahi et al. 1995; Baker & Hunstead 1995; Baker 1997).

2. DEFINITION OF THE MOLONGLO QUASAR SAMPLE

2.1. *MOST Observations*

The first step in forming a candidate quasar list was to reobserve all ~ 700 MRC sources with $S_{408} \geq 0.95$ Jy in the declination strip $-30° < \delta < -20°$ at 843 MHz with the Molonglo Observatory Synthesis Telescope (MOST) near Canberra, Australia (Robertson 1991). Each source, along with calibrators, was observed in a time-shared or "cuts" mode at several hour angles (Subrahmanya & Hunstead 1986; Hunstead 1991); the majority of observations were completed in 1986. The resulting images were CLEANed and restored with a Gaussian synthesized beam of typically $43'' \times 90''$. From these images, radio centroid positions were determined to about $1''$–$2''$ accuracy for unresolved or slightly resolved sources. The uncertainties are somewhat larger for sources that were confused or very extended.

2.2. *Optical Identifications*

Optical identifications were then sought close to the radio centroid positions on film copies of the UK Schmidt III-aJ sky survey, down to the limiting blue stellar magnitude of $b_{\rm J} \approx 22.5$. Only stellar counterparts were considered at this stage to be likely quasars. Optical positions with an rms accuracy of $\sim 0\farcs5$ were measured for all candidate objects that appeared, on the basis of transparent overlays, to be likely identifications. The measurements were made with the Bolton plate measuring machine at the University of Sydney, as described by Hunstead (1994). In order to limit the number of chance identifications, regions of right ascension at low Galactic latitudes ($|b| < 20°$) were excluded at this stage. We obtained an initial list of about 90 candidate quasars by looking for agreement in the optical and radio positions within $\sim$2–3 times the combined rms errors.

2.3. *Initial VLA Observations*

Images with better spatial resolution were needed to confirm the optical identifications for the quasar candidates. All sources in the strip with $b > 20°$ but excluding the R.A. range $14^{\rm h}03^{\rm m}$–$20^{\rm h}20^{\rm m}$ (apart from those already observed with the Very Large Array [VLA], e.g., VLA calibrators) were therefore imaged in snapshot mode with the VLA in New Mexico (see §§ 2.5 and 3). The first sets of observations were made at a frequency of 4.86 GHz, achieving a resolution of about $1''$. A full description of the VLA snapshot observations is given in § 3. These observations identified compact core components between two radio lobes in the vast majority of extended sources. In such cases, coincidence between the radio core and optical positions was used to check identifications. This both dramatically reduced the chance identification rate and overcame the inevitable systematic biases that can affect centroid positions. As a result, some 5% of the candidate quasar identifications were not supported by the VLA core positions.

2.4. *Optical Spectroscopy*

A program of optical spectroscopic observations of the quasar candidates was begun in 1989 with the 3.9 m Anglo-Australian Telescope (AAT) at Siding Spring Observatory, Australia. The RGO spectrograph and faint object red spectrograph (FORS) were used with the dichroic beam splitter to record the blue and red parts of the spectrum simultaneously, providing an overall wavelength coverage of typically 3400–10000 Å with spectral resolutions of 10–25 Å. Further details are given in Paper IV. The spectra were used to confirm the quasar nature of the identifications, the principal criterion being the presence of broad emission lines. A few faint narrow-line radio galaxies were excluded from the sample at this stage, as were a few bright (less likely) candidates that turned out to be Galactic stars.

The blue magnitudes ($b_{\rm J}$) of the quasars were obtained subsequently using the COSMOS/UKST Southern Sky Catalog (Yentis et al. 1992) available on line at the Anglo-Australian Observatory, as described in Baker (1994). The redshifts and optical magnitudes are listed here in Table 4 for completeness.

2.5. *Further Radio and Optical Imaging*

About 70% of the objects in our final quasar sample were identified through the procedures outlined above. The remaining 30% were obtained through observations of the parallel survey of all the remaining MRC sources (mainly radio galaxies) in the same declination strip (Paper I). This program was originally directed at finding radio galaxies at high redshift through the study of steep-spectrum radio sources (McCarthy et al. 1990, 1991), but its scope was subsequently enlarged to cover all sources in the region of the MRC selected for the quasar sample and thus to produce a large, uniformly selected sample. The observations used to find optical counterparts for this larger survey, including some quasars, are described below for completeness (see also Papers I and II).

Between 1989 and 1992, about 450 radio sources in the selected region of the MRC were imaged with the VLA at 4.86 GHz in snapshot mode with angular resolutions of $\sim 1''$–$5''$. This included almost all the MRC sources that had not already been observed as part of the earlier quasar program. Only 25 sources were not observed with the VLA because they were either already known to be identified with bright galaxies and had been imaged earlier with the VLA by Ekers et al. (1989) or were known to have a compact radio structure and were being used as VLA phase calibrators.

Deep optical imaging in the *r* band was then carried out for the majority of the 450 targets using either the 2.5 m du Pont telescope or, in the case of the brighter identifications, the 1 m Swope telescope at the Las Campanas Observatory in Chile. Details of the observing methods and data reduction are given in Paper I. To date, these observations have resulted in firm optical identifications for over 95% of sources in the whole strip, the vast majority being galaxies. However, about 30 of the sources appeared to have stellar counterparts and were therefore regarded as possible quasar candidates. Subsequent spectroscopic observations, made either with the NOAO 4 m telescope at Cerro Tololo in Chile or with the AAT, have confirmed most of them to be quasars. Closer examination shows that these sources were not included in the original list of quasar candidates for one or both of the following reasons:

1. Large positional differences (several arcseconds) between the optical positions and the MOST radio centroids. This was either because of the large angular sizes of the radio structures or confusion from nearby sources in the short-exposure MOST "snapshot" images.
2. Empty fields or plate limit counterparts on the UK Schmidt plates where star/galaxy separation is unreliable.

2.6. *The Final List*

Following this lengthy program of observations, a total of 105 quasars and six BL Lac objects were identified from the whole survey (five likely candidates still require spectroscopic confirmation; see Paper IV) forming the MQS. This gives a quasar fraction of about 20%, comparable with most other low-frequency surveys. The MQS is highly complete—we do not anticipate finding many more quasars in the strip as our spectroscopic survey nears completion. Also, it is considerably larger than the only other completely identified low-frequency selected sample, the 3CRR.

3. RADIO OBSERVATIONS

In this section, the VLA observations of the MQS are described and contour images are presented for all quasars with extended radio structures. Independent measurements of the radio core fluxes with the single-baseline Parkes-Tidbinbilla Interferometer (PTI) are also detailed.

3.1. *Journal of VLA Observations*

VLA observations were used to determine the radio structures of quasars in the sample and in the process to obtain accurate core positions (to $1''$) in order to make reliable optical identifications. To achieve both high angular resolution and high sensitivity to detect the cores, most of the observations were made in the 6 cm band in the BnA hybrid configuration (which is particularly suitable for southern hemisphere sources). Additional observations were made at 1.41 GHz (in CnB configuration) for some sources with large-scale structure and at 8.44 GHz (BnA configuration) for a few interesting sources of small angular extent.

TABLE 1

VLA Observation Log

Observing Session	Date of Observation	Array Configuration	Frequency (GHz)
a	1987 Oct 26	BnA	4.86
b	1987 Nov 6–7	BnA	4.86
c	1989 Feb 19	BnA	4.86
d	1990 Apr 20	BnA	8.44
e	1990 May 10	BnA	8.44
f...........	1990 Sep 18	BnA	4.86
g	1992 Feb 16	CnB	4.86
h	1993 May 24–27	CnB	1.41

The dates and VLA array configurations of all the observations made between 1987 October and 1993 May are given in Table 1. Each source was typically observed at one or two hour angles for between 3 and 7 minutes total duration. A phase calibrator was observed every 30 minutes. Flux calibration was based on observations of 3C 48 and 3C 286 using the flux density scale of Baars et al. (1977). The effective bandwidth of the observations was 100 MHz. Thirteen sources that were known VLA calibrators (see, e.g., Perley 1982) were not observed by us; most are known to be flat-spectrum core-dominated sources.

3.2. *Data Reduction and Radio Images*

The data were processed using standard AIPS software and techniques. Data from the two IF channels were combined to form 512 × 512 pixel images. The visibility phases were then self-calibrated using one or two iterations of the AIPS task SELFCAL. The final images have typical rms noise levels of between 0.1 and 0.3 mJy beam^{-1} and dynamic ranges (defined as the ratio of peak intensity to the rms noise value) of better than $\sim 200:1$ (see Table 2).

Contour plots of the 4.86 GHz radio images are presented in Figure 1 for quasars that were well resolved. The contours have been plotted at brightness levels corresponding to $L \times (-2, -1.4, -1, 1, 1.4, 2, 2.8, 4, 8, 16, 32, 64 \ldots)$ mJy beam^{-1}, where L has been chosen to be approximately 3 times the rms noise level. Table 2 lists L for each source along with the peak flux density in the image and the size and orientation of the elliptical Gaussian restoring beam. Additional contour plots for several sources at 1.41 or 8.44 GHz are presented in Figure 2.[2]

Morphological information and flux densities for all the sources imaged with the VLA are given in Table 3. For large, extended sources (generally with LAS $\gtrsim 30''$), some of the extended flux may have been missed in our snapshot observations for lack of short spacings. Flux density estimates for such sources are followed by a colon. A comparison of VLA flux densities with those listed in the recent Parkes-MIT-NRAO (PMN) catalog (Griffith et al. 1994) shows, however, that any missing flux is unlikely to exceed 5%–10%, except in one or two cases. PMN flux densities at

[2] Images of a number of other MQS sources at 1.41 or 8.44 GHz are not shown here because they were among data lost from a faulty backup tape. They will be published elsewhere.

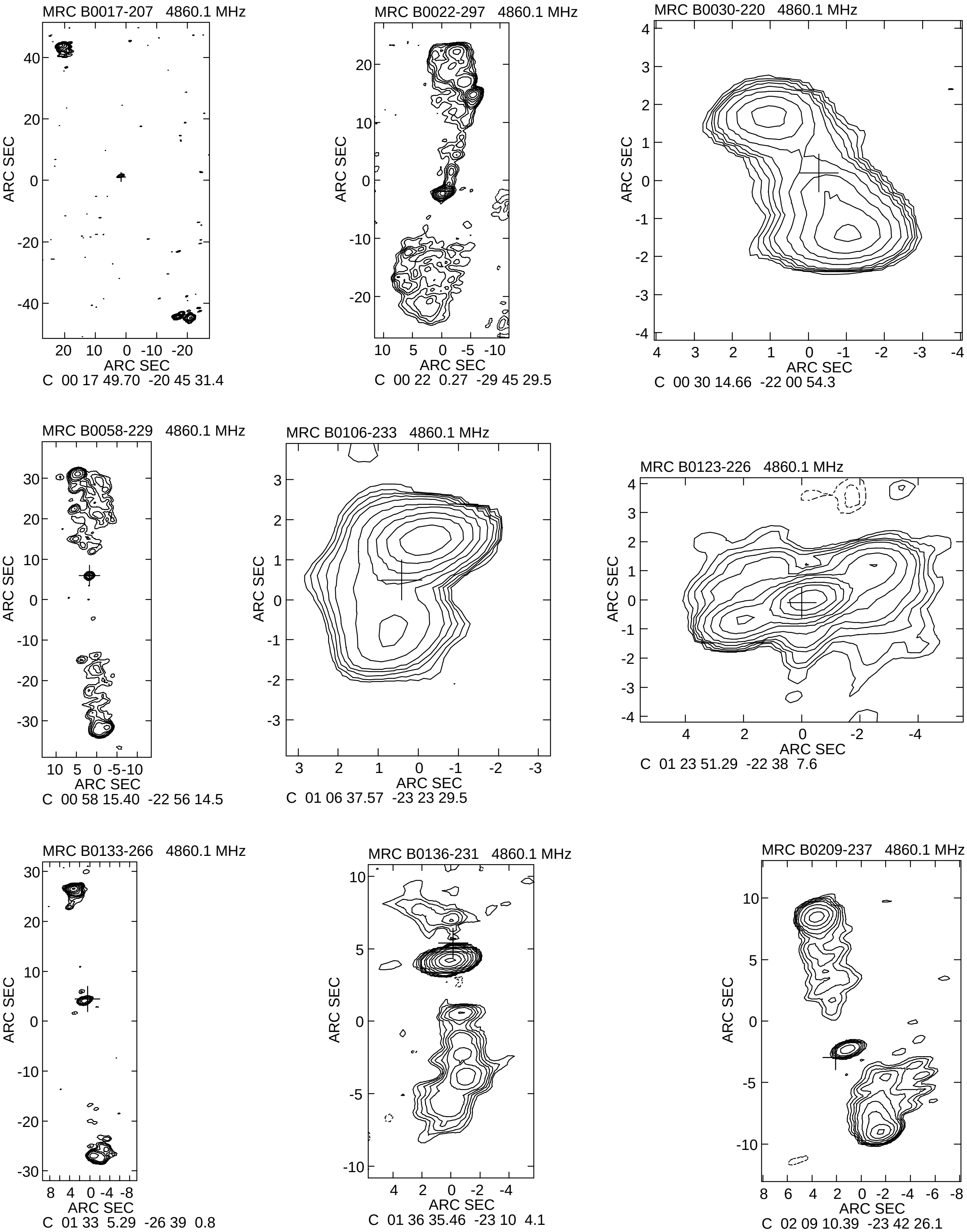

FIG. 1.—Contour plots from the VLA 4.86 GHz images of extended MQS sources. The B1950.0 position corresponding to the center of each image is listed below each plot. The contours levels plotted are $L \times (-2, -1.4, -1, 1, 1.4, 2, 2.8, 4, 8, 16, 32 \ldots)$, where the values of L in mJy beam^{-1} are listed in Table 2. The size and orientation of the elliptical Gaussian restoring beam in each case is listed in Table 2. The optical position of the quasar or BL Lac objects is marked with a cross; the size of the cross is chosen for convenience and does not reflect the error in the optical position.

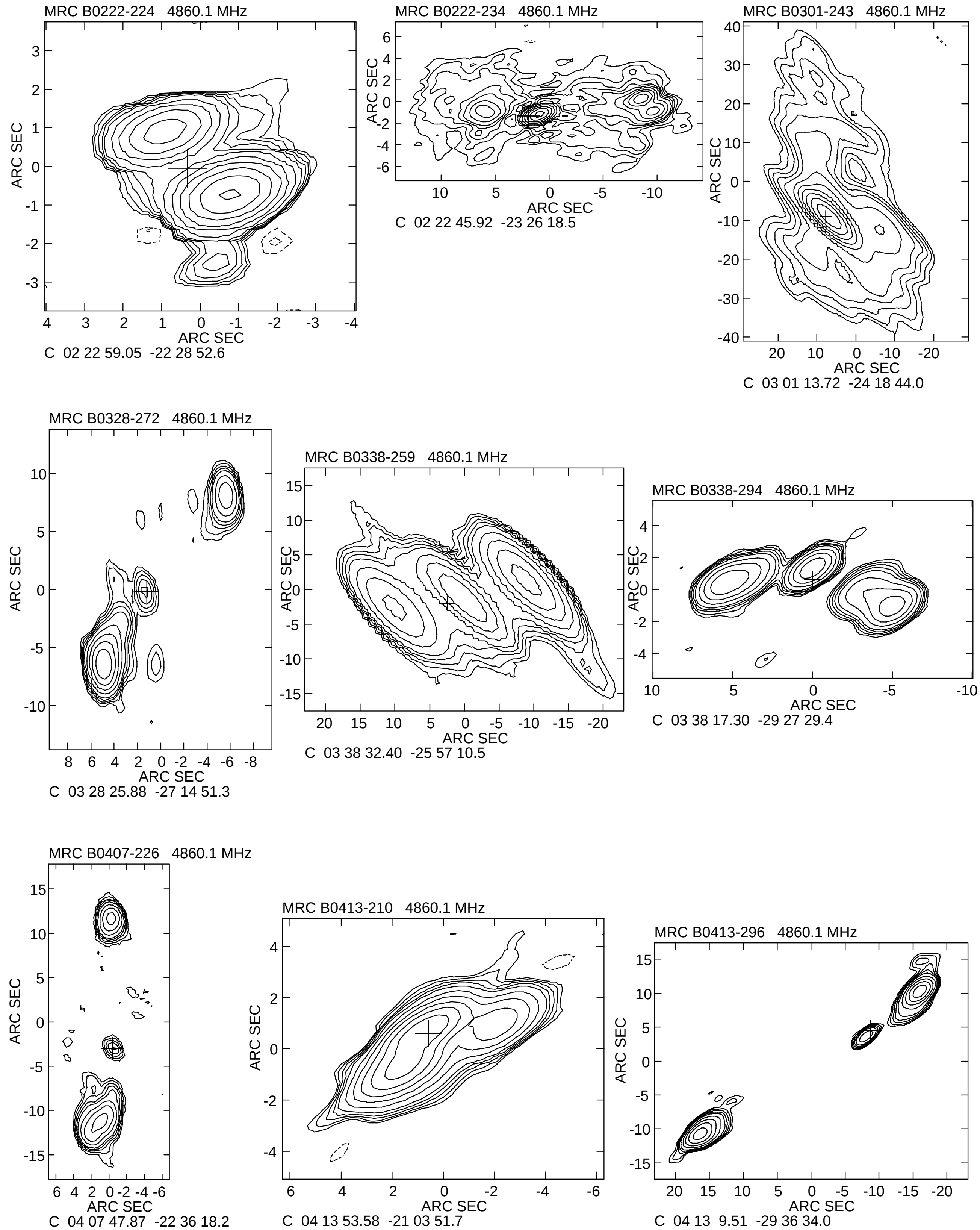

FIG. 1.—*Continued*

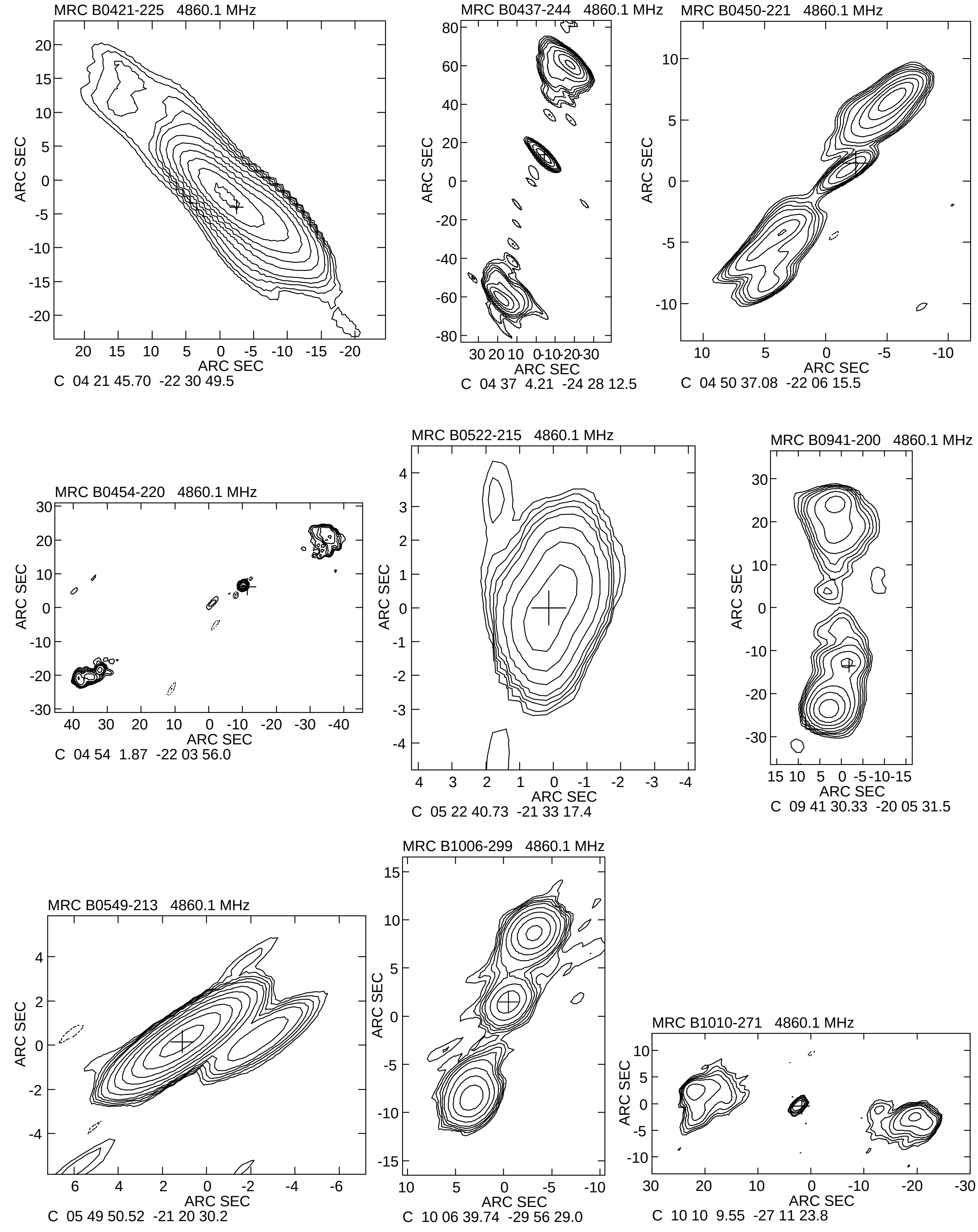

FIG. 1.—*Continued*

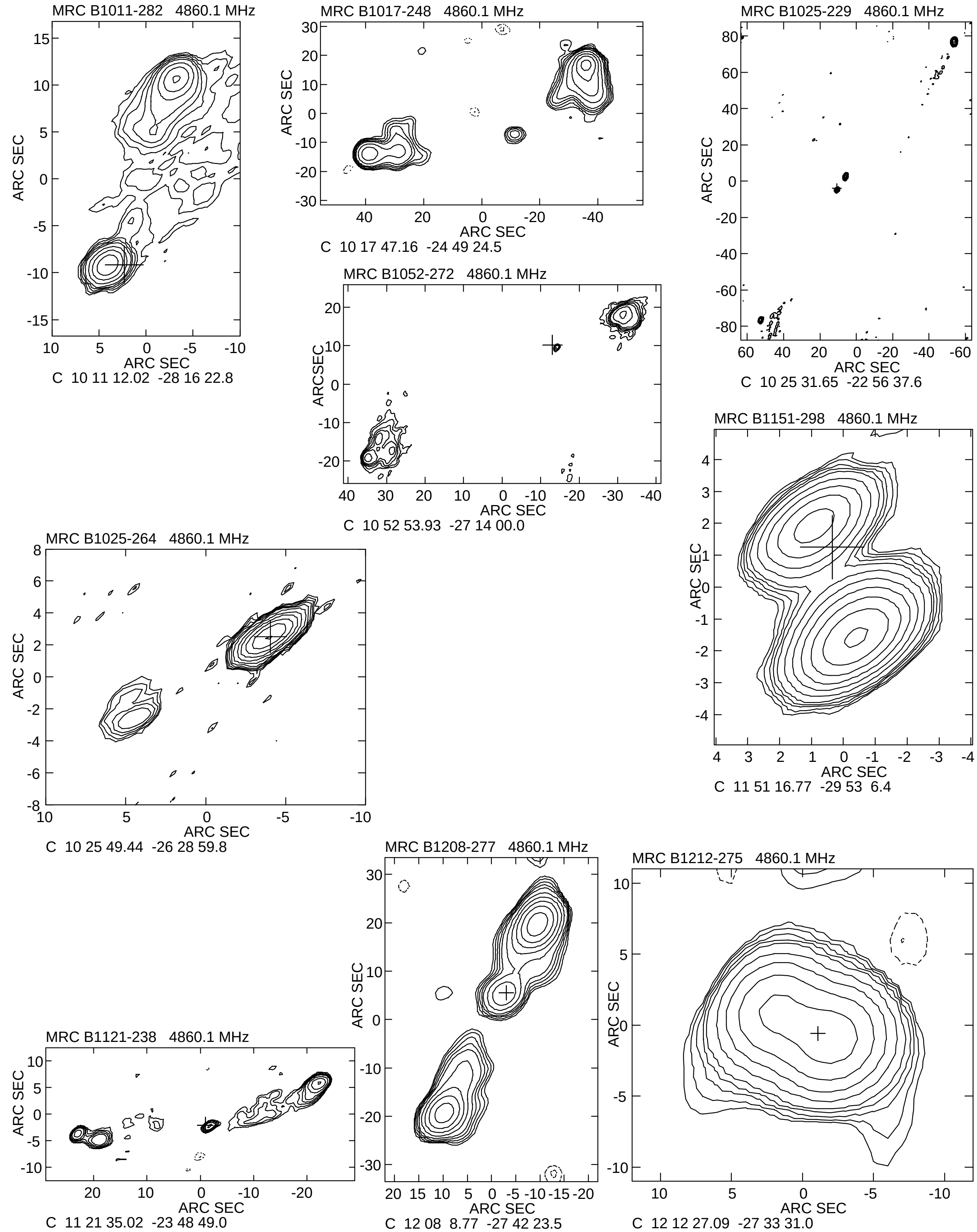

FIG. 1.—*Continued*

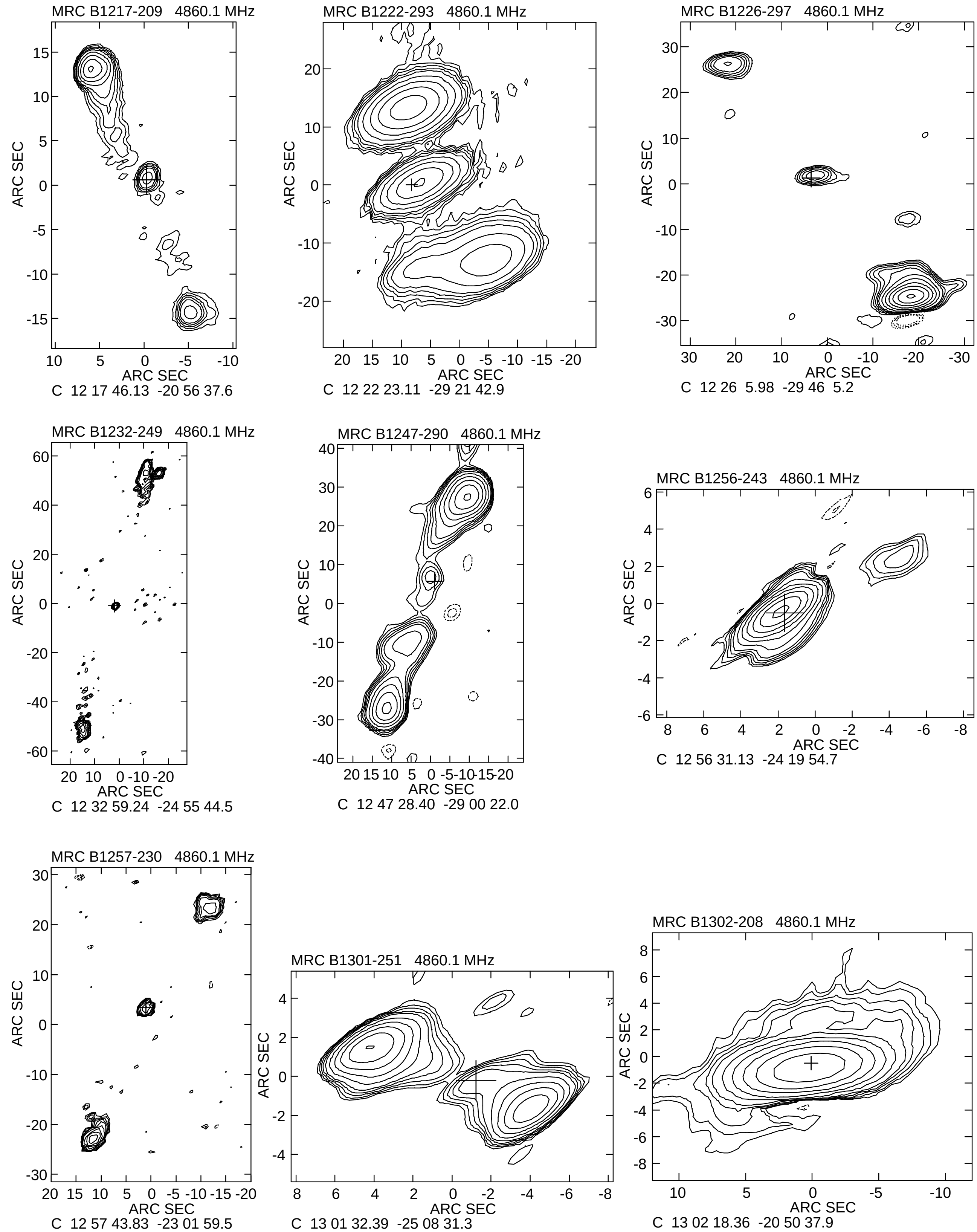

FIG. 1.—*Continued*

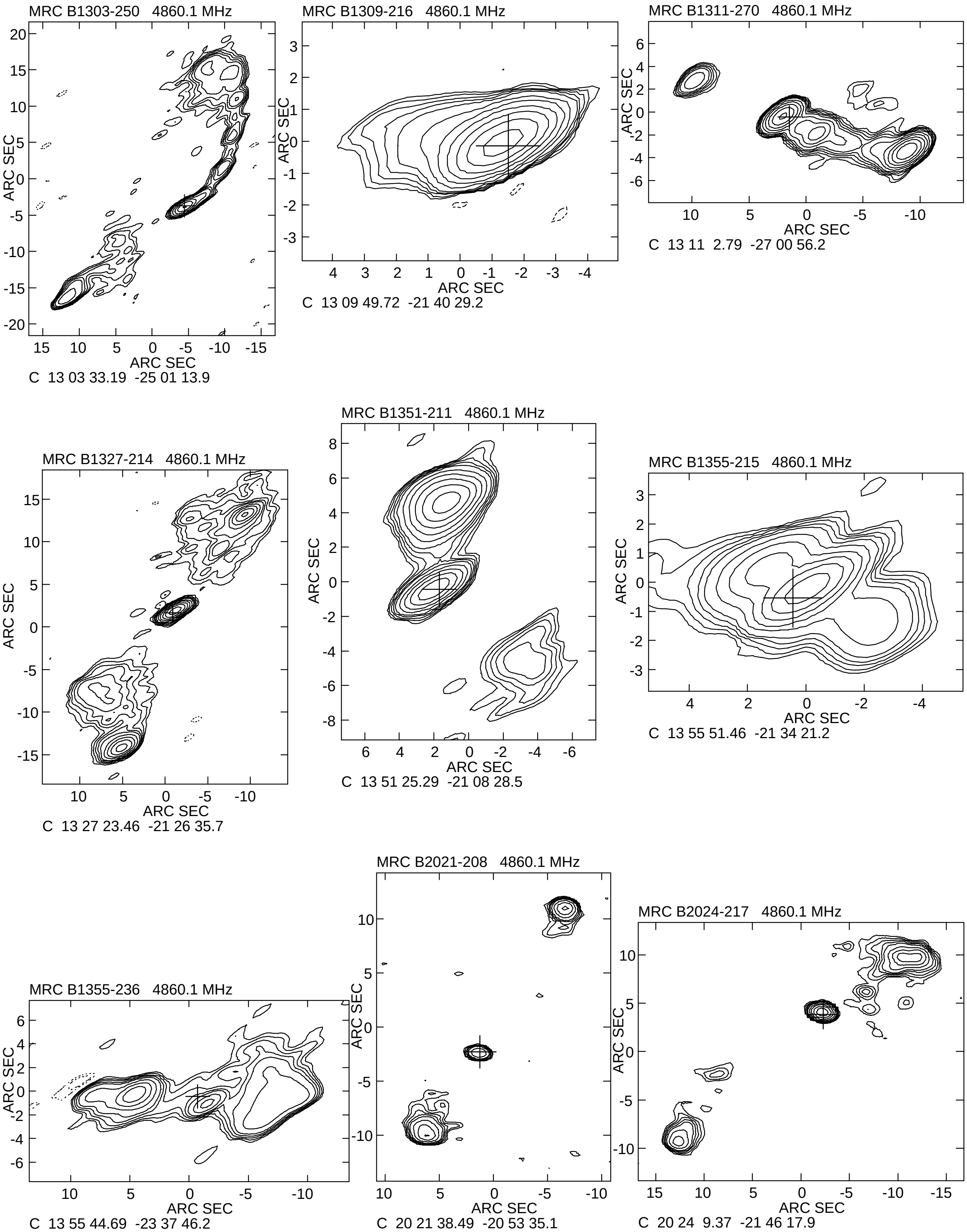

Fig. 1.—*Continued*

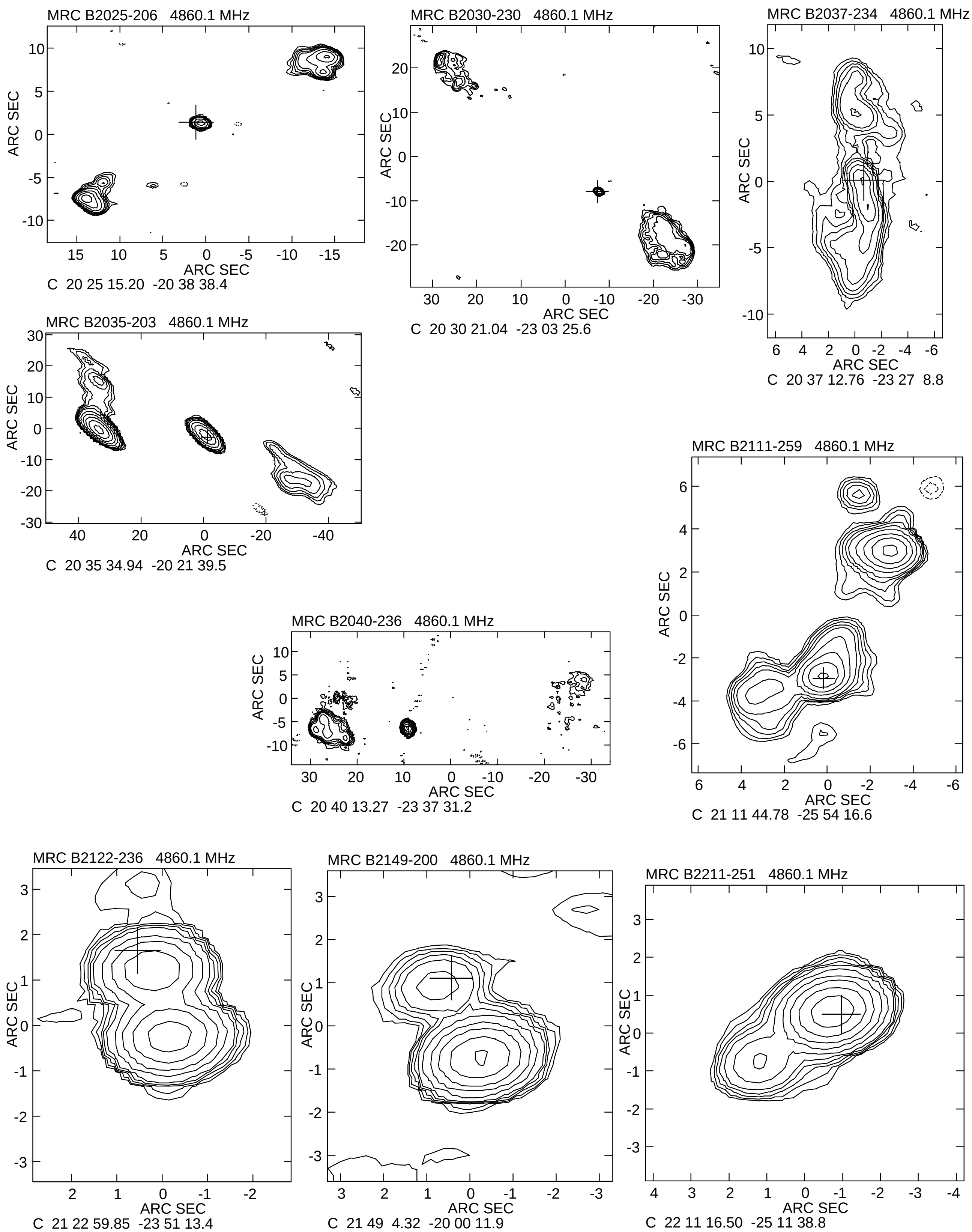

FIG. 1.—*Continued*

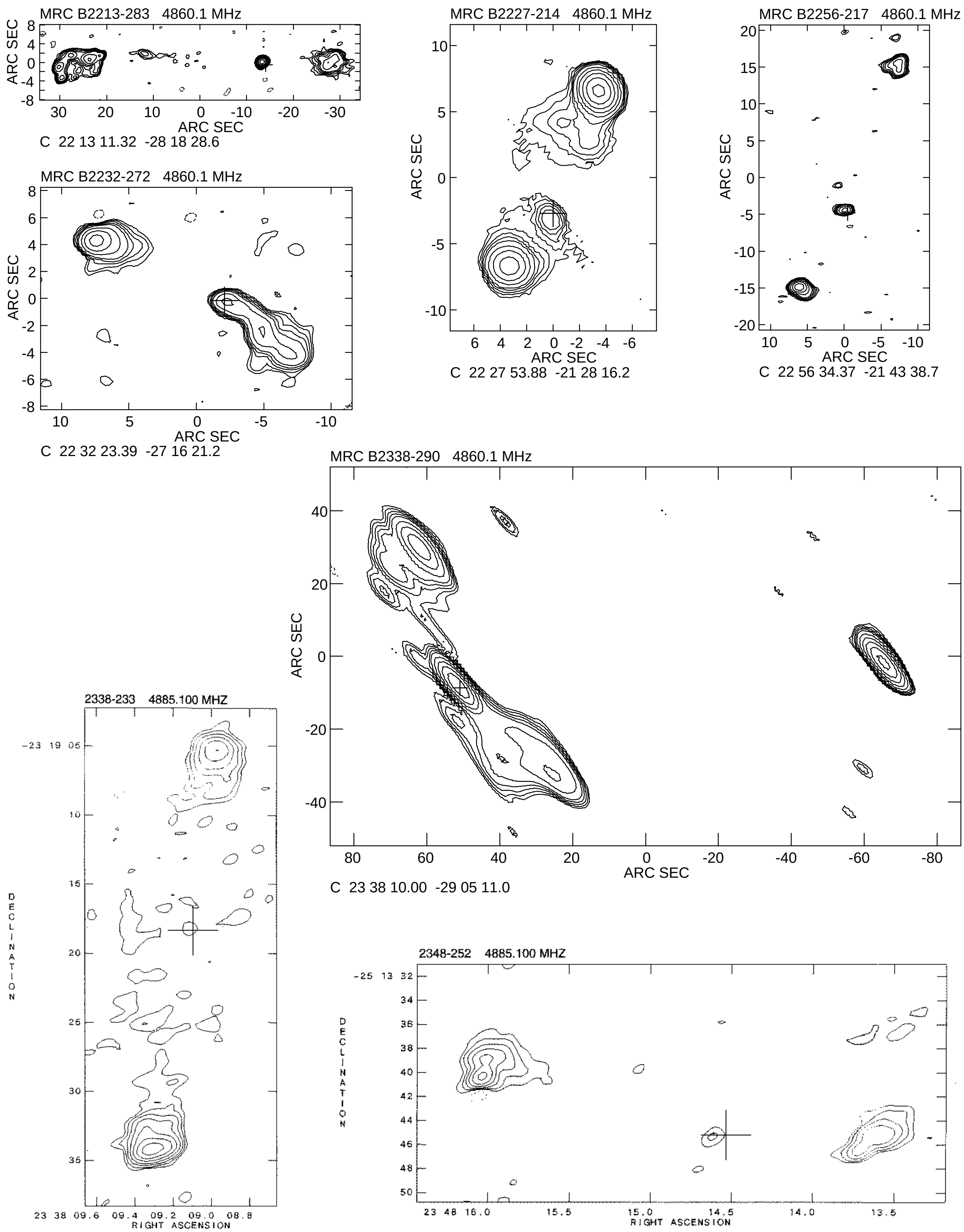

FIG. 1.—*Continued*

TABLE 2

VLA DATA FOR RESOLVED SOURCES SHOWN IN FIGURE 1

Source	$S_{4.86}$ (peak) (mJy beam^{-1})	Contour Level L (mJy beam^{-1})	Restoring Beam b_{maj} (arcsec)	b_{min} (arcsec)	PA (deg)
MRC B0017−207......	20.4	0.4	1.40	0.63	−80
MRC B0022−297......	125.0	1.2	1.38	0.94	−71
MRC B0030−220......	29.9	0.4	1.34	0.65	−84
MRC B0058−229......	8.8	0.4	1.75	1.24	−78
MRC B0106−233......	91.7	0.4	1.36	0.68	−81
MRC B0123−226......	233.6	0.5	1.39	0.67	−79
MRC B0133−266......	29.0	0.4	1.35	0.76	−77
MRC B0136−231......	250.0	0.4	1.34	0.68	−83
MRC B0209−237......	28.2	0.4	1.45	0.69	−75
MRC B0222−234......	158.0	1.0	1.47	0.76	−72
MRC B0222−224......	145.7	0.5	1.47	0.72	−74
MRC B0301−243......	228.4	0.5	9.25	3.00	45
MRC B0328−272......	62.2	0.5	2.44	1.19	7
MRC B0338−294......	24.7	0.4	2.01	1.03	−56
MRC B0338−259......	33.7	0.4	9.50	2.50	45
MRC B0407−226......	17.1	0.4	1.65	1.24	28
MRC B0413−296......	71.7	0.7	2.64	1.20	−52
MRC B0413−210......	510.4	2.0	2.11	0.78	−61
MRC B0421−225......	152.9	0.5	9.50	2.75	45
MRC B0437−244......	23.3	0.3	10.75	2.75	45
MRC B0450−221......	63.7	0.6	2.78	0.89	−57
MRC B0454−220......	151..2	2.0	1.39	1.31	−41
MRC B0522−215......	69.1	1.5	2.03	1.21	12
MRC B0549−213......	181.3	0.5	3.36	0.86	−56
MRC B0941−200......	40.7	0.4	5.00	4.00	90
MRC B1006−299......	55.7	0.7	3.08	2.32	−47
MRC B1010−271......	11.7	0.6	2.68	1.82	−50
MRC B1011−282......	61.4	1.0	2.51	1.93	−49
MRC B1017−248......	25.6	0.3	4.75	4.50	90
MRC B1025−229......	11.3	0.5	1.64	1.21	−27
MRC B1025−264......	262.2	1.0	2.28	0.93	−57
MRC B1052−272......	9.1	0.5	1.81	1.26	−23
MRC B1121−238......	16.7	0.5	1.81	1.11	−62
MRC B1151−298......	113.7	0.4	2.13	1.12	−54
MRC B1208−277......	83.0	0.4	5.00	4.00	−45
MRC B1212−275......	49.3	0.5	4.75	4.25	−45
MRC B1217−209......	28.3	0.4	1.67	1.25	−24
MRC B1222−293......	65.9	0.7	8.22	3.75	−65
MRC B1226−297......	111.8	0.4	5.29	2.53	−83
MRC B1232−249......	83.0	1.5	1.46	1.40	−42
MRC B1247−290......	67.5	0.5	5.00	4.25	−45
MRC B1256−243......	358.2	1.2	2.28	0.89	−57
MRC B1257−230......	69.9	0.8	1.48	1.44	−43
MRC B1301−251......	52.4	0.4	2.20	0.87	−57
MRC B1302−208......	235.4	1.0	5.30	1.99	−82
MRC B1303−250......	33.3	0.5	2.11	0.87	−58
MRC B1309−216......	141.9	0.4	1.93	0.75	−62
MRC B1311−270......	102.4	0.4	1.95	1.02	−56
MRC B1327−214......	197.6	1.0	1.95	0.77	−62
MRC B1351−211......	75.5	0.4	2.22	0.81	−59
MRC B1355−215......	139.2	0.7	2.07	0.76	−60
MRC B1355−236......	23.5	0.4	2.07	0.81	−59
MRC B2021−208......	18.5	0.5	1.30	0.74	84
MRC B2024−217......	67.3	0.6	1.29	0.83	81
MRC B2025−206......	21.8	0.4	1.29	0.75	80
MRC B2030−230......	20.5	1.2	1.32	0.90	68
MRC B2035−203......	166.1	1.0	6.75	2.75	48
MRC B2037−234......	13.7	0.4	1.44	0.99	28
MRC B2040−236......	89.5	0.6	1.59	1.18	23
MRC B2111−259......	151.3	2.0	1.24	0.92	−89
MRC B2122−236......	95.1	1.0	1.26	0.81	−90
MRC B2149−200......	408.5	3.0	1.26	0.79	−85
MRC B2211−251......	165.6	0.8	1.29	0.93	−79
MRC B2213−283......	47.8	0.5	1.28	1.05	−73
MRC B2227−214......	79.3	0.5	1.68	1.45	30
MRC B2232−272......	22.7	0.5	1.26	0.92	−77
MRC B2256−217......	16.3	0.3	1.27	0.76	−82
MRC B2338−233......	29.9	0.3	1.36	0.82	−74
MRC B2338−290......	66.2	0.4	9.25	2.75	40
MRC B2348−252......	60.1	1.5	1.40	0.85	−70

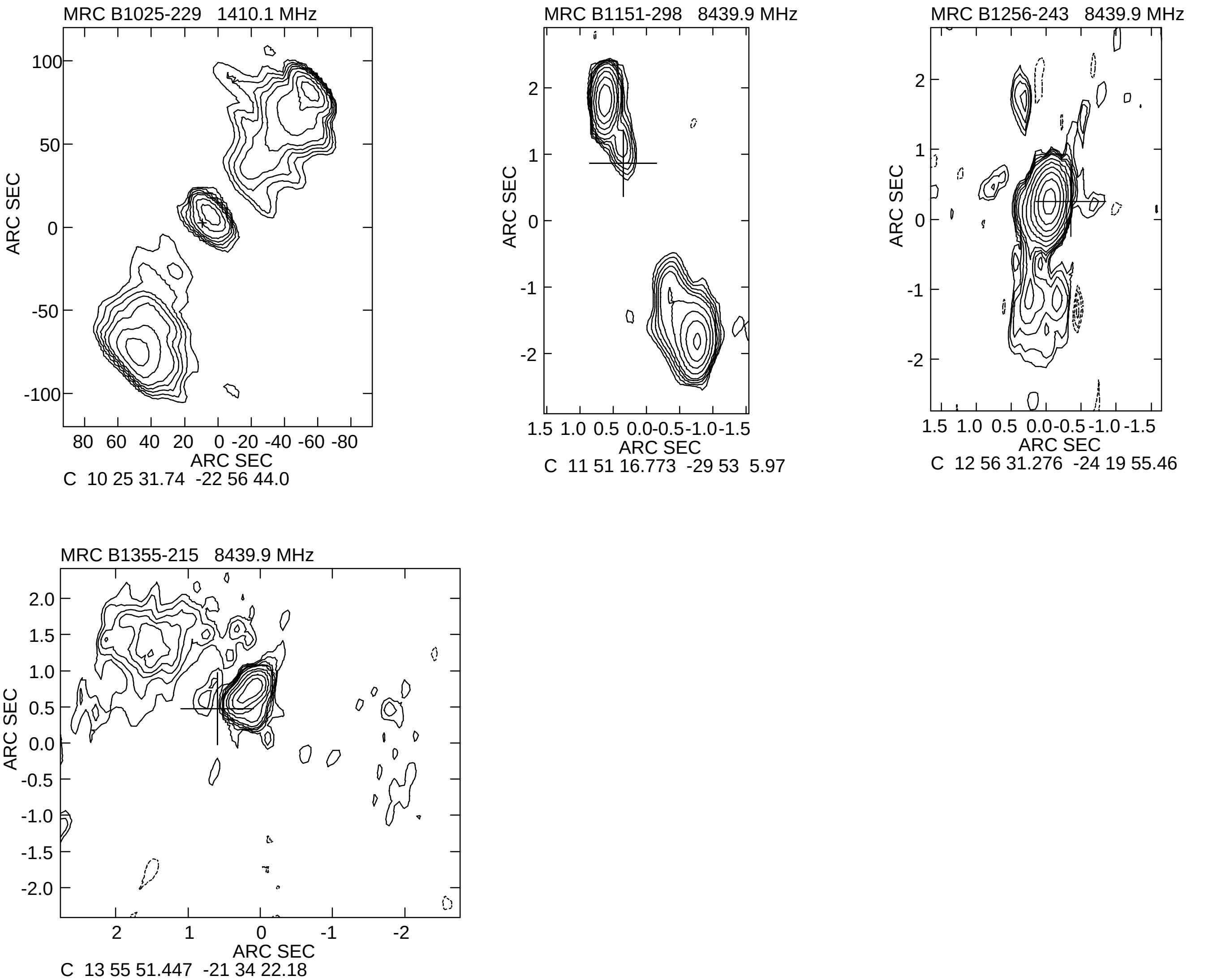

FIG. 2.—VLA contour images of some sources at 8.4 or 1.4 GHz. The first contour levels (L) and restoring beam sizes are as follows: MRC B1025−229: 1.5 mJy beam^{-1}, 16″.8 × 7″.0 (40°); MRC B1151−298: 0.4 mJy beam^{-1}, 0″.46 × 0″.19 (−60°); MRC B1256−243: 1.0 mJy beam^{-1}, 0″.52 × 0″.24 (−4°); MRC B1355−215: 0.4 mJy beam^{-1}, 0″.24 × 0″.18 (−29°). The contours levels plotted are $L \times (-2, -1.4, -1, 1, 1.4, 2, 2.8, 4, 8, 16, 32 \ldots)$.

4.86 GHz are listed in Table 3 for the 13 sources that are known VLA calibrators and were not reobserved under this program. Measurements of the largest angular size (LAS) of the sources have been made between the brightest peaks (generally hot spots) in the two lobes.

3.3. *High-Resolution Observations with the Parkes-Tidbinbilla Interferometer*

Isolated radio cores were clearly detected in most of the extended quasars in the VLA observations. However, with 1″ resolution it was not always clear if all the observed flux density in this component was being contributed by a true subparsec-scale "core" or whether it was partly contaminated by flux from parts of jets or nearby lobes. This was particularly true for small sources with extents of a few arcseconds. In order to get a better estimate of the core flux densities on angular scales of ∼0″.1, most of the sources were also observed with the two-element Parkes-Tidbinbilla Interferometer (PTI). The PTI uses the 64 m dish at Parkes with either the 70 m or 34 m dish at Tidbinbilla, over a baseline of 275 km (Norris et al. 1988).

Observations of 95 sources were made at a frequency of 2.29 GHz in 1993 January 22–25 using the Parkes telescope as one of the elements and (mostly) the 70 m dish at Tidbinbilla. Typical integration times were about 5 minutes per source, each observed at a single hour angle, yielding an rms noise level of ∼1 mJy. Hydra A and 1934−638 were observed as primary calibrators. The data were reduced at the University of Sydney using the ATLOOK software (Norris 1989); additional details are given in Baker (1994). For those sources observed, derived PTI flux densities on scales ≲0″.1 are listed in Table 3 along with the core flux densities measured from the VLA images.

The 4.86 GHz core flux density from the VLA is plotted against the PTI flux density in Figure 3. There is good agreement, particularly at $S_{4.86}$(core) ≳ 10 mJy. This shows that the PTI measurements are not significantly affected by fringe-beating effects (which could result from observing compact structure in the source at a single hour angle and on a single baseline), except possibly in a handful of cases. The few sources where the PTI flux is significantly larger than the VLA value all have small angular sizes (LAS ≲

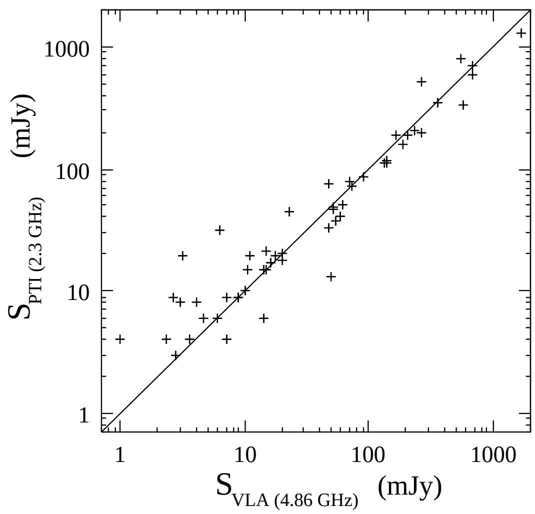

FIG. 3.—Plot of the correlated flux densities from the Parkes-Tidbinbilla Interferometer at 2.29 GHz against the VLA core flux densities at 4.86 GHz.

10″) and compact structure in the lobes that could be responsible for the discrepancy. Variability in the cores could also play a part, as could core spectral indices which differ significantly from $\alpha_{core} \sim 0$. Figure 3 shows, however, that the average spectral index of radio cores between 2.29 and 4.86 GHz is close to zero. Thus, the PTI observations are most useful in assessing the reliability of VLA core fluxes and in clarifying the compact structures in several cases.

3.4. *Radio and Optical Properties*

Further radio and optical properties of the MQS are tabulated in Tables 3 and 4. For estimates of intrinsic radio power and linear size we have used $H_0 = 50$ km s^{-1} Mpc^{-1} and $q_0 = 0.5$ throughout.

For sources with clear cores, we have calculated the parameter R_{10}, which is the ratio of the core flux density to the extended lobe flux density at a rest frequency of 10 GHz. This rest frequency was chosen to minimize spectral index corrections at the median redshift of the sample $z \approx 1$. R_{10} is defined by

$$R_{10} = \frac{S_c\{[4.86(1+z)]/10\}^{\alpha_c}}{S_e\{[4.86(1+z)]/10\}^{\alpha_e}} ,$$

where S_c and S_e are the observed flux densities of the radio core and the extended emission at 4.86 GHz, and α_c and α_e are the spectral indices for the core and extended emissions, respectively. In the absence of definite information on the spectral indices, we have assumed $\alpha_c = 0$ and $\alpha_e = 0.9$, which are typical values for cores and lobes, respectively. R_{10} is commonly used as an orientation indicator (see, e.g., Orr & Browne 1982). We define lobe-dominated sources to have $R_{10} < 1$ and core-dominated sources to have $R_{10} \geq 1$. The ratio R_{10} has not been estimated for compact steep-spectrum (CSS) sources in the sample, i.e., intrinsically small radio sources with $\alpha > 0.5$ and linear sizes $\lesssim 20$ kpc, nor for gigahertz-peaked spectrum (GPS) sources. For core-dominated quasars that were not observed by us with the VLA, lower limits to R_{10} have been estimated based on the observations of Perley (1982), on information in the VLA calibration book, and on a decomposition of the overall radio spectrum into core and extended components whenever possible.

Table 3 is arranged as follows:

Column (1).—Source name (IAU designation).

Column (2).—Total flux density at 408 MHz as listed in MRC.

Column (3).—VLA integrated flux density at 4.86 GHz. A colon following the entry indicates that some flux may have been missed in the snapshot observations. Entries marked with an asterisk are 4.86 GHz flux densities from the PMN catalog; these sources are VLA calibrators and were not reobserved in this program.

Column (4).—Spectral index between 408 MHz and 4.86 GHz, $\alpha_{0.408}^{4.86}$; ($S_\nu \propto \nu^{-\alpha}$).

Column (5).—VLA core flux density at 4.86 GHz.

Column (6).—PTI correlated flux density at 2.29 GHz.

Column (7).—Ratio of core to lobe flux density at an emitted frequency of 10 GHz; CSS = compact steep-spectrum source; GPS = gigahertz peaked-spectrum source.

Column (8).—Morphological type of the radio structure:

T = triple; lobes on either side of a radio core.

D = double, without a well-defined or resolved radio core.

D2 = an extended component on only one side of the radio core.

CJ = core-jet structure.

R = resolved.

U = unresolved.

Column (9).—Largest angular size (LAS).

Column (10).—Ratio of the integrated 4.86 GHz flux density in the weaker to the stronger lobe. The suffix n (north), s (south), e (east), or w (west) identifies the weaker lobe.

Column (11).—Code identifying the observing session as listed in Table 1. "N" indicates additional notes in Section 4.

Table 4 is arranged as follows:

Column (1).—Source name (IAU designation).

Columns (2) and (3).—VLA core radio position (B1950) measured either at 4.86 or 8.41 GHz. For unresolved or marginally resolved sources, the positions refer to the radio centroid. In a few sources without a detected core, the position given is that of the midpoint of the extended components (see additional notes on individual sources).

Columns (4) and (5).—Optical position (B1950), typically accurate to 0″.5–1″. For brevity, only seconds of R.A. and arcseconds of decl. are given.

Column (6).—Reference code for the optical position:

1 = Sydney University measurement.

2 = APM.

3 = COSMOS with first-order correction (see Drinkwater, Barnes, & Ellison 1995).

4 = COSMOS raw value.

5 = measured from our CCD images using the coordinates of stars from the digitized III-aJ plates at STScI as reference (these have rms errors ~1″).

Column (7).—Blue magnitude, b_J, as recorded in the COSMOS database. Red r-band CCD magnitudes are given with an r suffix for three quasars too faint to be detected on the blue survey plates.

Column (8).—Spectroscopic redshift.

TABLE 3

Radio Data for the Molonglo Quasar Sample

Source (1)	$S_{0.408}$(Jy) (2)	$S_{4.86}$ (total) (mJy) (3)	$\alpha_{0.408}^{4.86}$ (4)	$S_{4.86}$ (core) (mJy) (5)	$S_{2.29}$ (PTI) (mJy) (6)	R_{10} (7)	Morphological Type (8)	LAS (arcsec) (9)	Lobe Flux Ratio (10)	Observing Code; Notes (11)
MRC B0017−207......	1.25	120:	0.95:	2.8	<3	0.031	T	96	0.74s	b
MRC B0022−297......	7.83	905:	0.87:	134	111	0.22	T	44	0.56s	b; N
MRC B0029−271......	1.21	111	0.96	...	11	CSS	U	≲1	...	b
MRC B0030−220......	1.01	101	0.93	...	14	0.150	T	3.9	0.6n	b, e; N
MRC B0040−208......	1.12	121	0.90	...	41	CSS	U	≲2	...	f, h
MRC B0058−229......	1.24	118:	0.95:	2.3	<4	0.024	T	63	0.75s	b
MRC B0106−233......	1.13	138	0.85	...	25	<0.25	D	2.5	0.33s	b, e; N
MRC B0111−256......	0.98	182	0.68	...	...	CSS	R	2.2	...	g; N
MRC B0118−272......	1.40	1000∗	0.07	...	652	...	U	...	...	N
MRC B0123−226......	1.54	365	0.58	234	209	2.10	T	5.1	0.80w	b, e; N
MRC B0133−266......	1.19	107:	0.97:	14	15	0.12	T	53.5	0.61s	b
MRC B0135−247......	2.20	956∗	0.37	...	710	>2	U	...	...	...
MRC B0136−231......	1.30	339	0.54	260	197	2.14	T	12.8	0.23n	b
MRC B0142−278......	1.01	690	0.15	690	692	>5	U	<1	...	b
MRC B0209−237......	1.50	155	0.92	6	6	0.049	T	18.0	0.73n	b
MRC B0222−234......	5.44	770	0.79	186	160	0.50	T	15.5	0.48e	b
MRC B0222−224......	2.36	227	0.95	...	43	<0.37	D	2.4	0.33n	b, e; N
MRC B0237−233......	3.67	3630∗	0.05	...	4600	GPS	U	...	...	N
MRC B0246−231......	2.44	430	0.70	...	245	CSS	U	<1	...	b
MRC B0301−243......	1.35	360	0.53	228	...	...	R	60:	...	g; N
MRC B0315−282......	1.00	288	0.52	...	...	CSS	R	≲2	...	g; N
MRC B0327−241......	1.24	866∗	0.18	...	425	>1	U	...	...	...
MRC B0328−272......	1.06	123	0.87	2.7	9	0.017	T	18.1	0.19n	f
MRC B0338−294......	1.03	106	0.92	23	45	0.27	T	10.5	0.94w	b; N
MRC B0338−214......	1.26	894	0.14	...	...	...	U	≲1	...	g; N
MRC B0338−259......	1.06	111	0.91	25	...	...	T	19.7	0.54e	g; N
MRC B0346−279......	1.11	1444∗	0.17	...	846	>5	U	...	...	...
MRC B0407−226......	1.24	100	1.01	1.5	...	0.013	T	23.1	0.50n	c
MRC B0413−296......	3.71	262	1.07	10	10	0.031	T	39.0	0.97w	b
MRC B0413−210......	7.30	1193	0.73	510	...	0.71	T	5.0	...	b, e; N
MRC B0418−288......	1.16	108	0.96	...	...	CSS	U	<2	...	g
MRC B0421−225......	1.72	250	0.78	...	...	...	R	8.1	...	g; N
MRC B0430−278......	0.95	146	0.76	...	...	CSS	U	<2	...	f
MRC B0437−244......	1.28	129	0.93	10.5	15	0.098	T	126	0.53s	g
MRC B0439−299......	1.10	289	0.54	...	...	CSS	U	<2	...	g; N
MRC B0447−230......	0.96	122	0.83	...	...	CSS	U	<2	...	f
MRC B0450−221......	3.23	206	1.11	15	21	0.086	T	14.3	0.56s	b
MRC B0451−282......	2.14	2172∗	0.06	...	2395	>5	U	...	...	...
MRC B0454−220......	4.93	715:	0.78:	168	187	0.39	T	84	0.77w	b
MRC B0522−215......	1.75	149	1.00	...	34	...	R	2.5	...	f; N
MRC B0549−213......	1.70	219	0.83	...	98	<0.55	D2	3.6	...	b; N
MRC B0925−203......	1.36	689∗	0.15	...	526	>3	U	...	...	...
MRC B0941−200......	1.03	115	0.88	≲7	<4	<0.08	T	47.7	0.5n	g
MRC B1006−299......	1.44	140	0.94	20	20	0.166	T	18.3	0.69s	a
MRC B1010−271......	1.42	95:	1.09:	3.6	<4	0.058	T	44.3	0.95e	a
MRC B1011−282......	2.60	197:	1.04:	59	41	≲0.76	T	64	0.2s	a; N
MRC B1017−248......	0.95	89	0.95	1.1	...	...	T	79.8	0.36e	g; N
MRC B1019−227......	0.96	85	0.98	...	27	CCS	D	2.2	0.67?	c; N
MRC B1025−229......	1.05	58:	1.17:	10	...	0.15:	T	188	0.74n	c, h; N
MRC B1025−264......	1.53	318	0.63	265	514	5.61	D2	10.2	...	a, h; N
MRC B1043−291......	1.09	680	0.19	680	588	>5	U	<1	...	a
MRC B1052−272......	2.05	145	1.07	1.4	...	0.01	T	76.5	0.88e	c
MRC B1055−242......	1.95	562∗	0.51	...	328	>1	U	...	...	...
MRC B1106−227......	1.81	300	0.73	...	81	CSS	U	<1	...	a
MRC B1114−220......	1.61	270	0.72	...	90	CSS	U	<1	...	a
MRC B1117−248......	2.69	736∗	0.54	...	796	CSS	U	...	...	...
MRC B1121−238......	1.57	107:	1.09:	4	8	0.049	T	46.0	0.50e	a
MRC B1151−298......	1.44	177	0.85	...	41	0.013	T	4.0	...	a, d; N
MRC B1156−221......	2.66	570∗	0.61	...	...	CSS	U	...	...	...
MRC B1202−262......	3.55	950	0.53	580	332	1.78	T	15	0.54e	a, h; N
MRC B1208−277......	1.58	202	0.83	15	15	0.088	T	43.4	0.48s	g
MRC B1212−275......	0.96	89	0.96	...	...	...	R	3.5	...	g; N
MRC B1217−209......	1.00	97	0.94	4.7	<6	0.057	T	29.8	0.34s	c
MRC B1222−293......	1.33	201	0.76	52	48	0.38	T	29.4	0.52s	f; N
MRC B1224−262......	3.18	401	0.83	...	...	CSS	U	<2	...	g
MRC B1226−297......	1.20	150	0.84	3.1	<19	0.024	T	64.5	0.05n	f
MRC B1232−249......	5.10	650:	0.83:	16	17	0.036	T	109	0.79s	a
MRC B1244−255......	1.23	2317∗	0.13	...	1540	>5	U	...	...	...
MRC B1247−290......	1.87	198	0.91	3	...	0.018	T	57.6	0.64s	g
MRC B1256−220......	1.06	978∗	0.12	...	700	>3	U	...	...	...

TABLE 3—*Continued*

Source (1)	$S_{0.408}$(Jy) (2)	$S_{4.86}$ (total) (mJy) (3)	$\alpha^{4.86}_{0.408}$ (4)	$S_{4.86}$ (core) (mJy) (5)	$S_{2.29}$ (PTI) (mJy) (6)	R_{10} (7)	Morphological Type (8)	LAS (arcsec) (9)	Lobe Flux Ratio (10)	Observing Code; Notes (11)
MRC B1256−243......	1.00	403	0.37	358	352	>3	T	8.2	...	a, d; N
MRC B1257−230......	3.23	242:	1.05:	18	<19	0.078	T	52	0.3n	a
MRC B1301−251......	1.16	163	0.79	3:	<19	0.020	T	8.7	0.71w	a
MRC B1302−208......	1.39	285	0.62	...	...	...	R	2.6	...	f; N
MRC B1303−250......	1.51	190:	0.80:	38	...	0.23	T	38.5	0.59e	a; N
MRC B1309−216......	1.03	185	0.69	140	115	...	CJ	3	...	a; N
MRC B1311−270......	1.77	235	0.82	61	50	0.24	T	19.5	0.07e	a; N
MRC B1327−214......	5.63	747:	0.82:	208	191	0.49	T	31.0	0.76n	a
MRC B1348−289......	0.97	250	0.54	...	...	CSS	U	<2	...	g; N
MRC B1349−265......	3.59	752	0.63	...	424	CSS	U	<2	...	g
MRC B1351−211......	2.29	223	0.94	47	33	0.23	T	11	0.1s	a; N
MRC B1355−236......	1.44	138	0.95	11	<19	0.098	T	16	0.88e	a
MRC B1355−215......	1.87	257	0.80	139	113	0.84	T	4.2	0.3w	a, d; N
MRC B1359−281......	2.30	640	0.52	...	444	CSS	R	1.4	...	a; N
MRC B2021−208......	1.65	93:	1.16:	9	9	0.099	T	24.5	0.66n	b
MRC B2024−217......	2.45	275:	0.88:	72	72	0.48	T	31.0	0.36e	b
MRC B2025−206......	1.94	120:	1.12:	9	9	0.068	T	32.5	0.85e	b
MRC B2030−230......	6.45	545:	1.00:	20	18	0.037	T	70	0.45e	b
MRC B2035−203......	1.87	276	0.77	50	13	≲0.28	T	64	0.14w	g; N
MRC B2037−234......	0.96	95	0.93	14	6	0.16	T	15	0.38n	c
MRC B2040−236......	1.05	228	0.61	92	87	0.76	T	56	0.47w	c
MRC B2059−214......	1.50	305	0.64	...	...	CSS	R	2.2	...	g; N
MRC B2111−259......	5.27	560	0.91	145:	99	0.26	T	9.0	...	b, e; N
MRC B2122−238......	1.05	180	0.71	69	80	0.50	D2	1.6	...	b, e; N
MRC B2128−208......	6.15	559	0.97	...	...	CSS	U	<2	...	g
MRC B2136−251......	1.20	291	0.57	...	173	CSS	U	<2	...	f, h; N
MRC B2149−200......	5.12	550	0.90	47	76	0.13	D2	2.0	...	b, e; N
MRC B2156−245......	1.39	160	0.87	...	127	CSS	U	<2	...	g
MRC B2158−206......	1.15	132	0.87	...	84	CSS	U	<1	...	b
MRC B2210−257......	1.61	823*	0.18	...	...	>3	U	...	...	...
MRC B2211−251......	2.30	203	0.98	...	...	?	D2?	2.4	...	b; N
MRC B2213−283......	2.54	225:	0.98:	52	46	0.32	T	58	0.70w	b
MRC B2227−214......	1.81	152	1.00	3	8	0.017	T	15.1	0.40s	c
MRC B2232−272......	1.11	123	0.89	10:	<5	≲0.074	T	16	0.93e	b, e; N
MRC B2240−260......	1.57	630	0.15	560	800	>5	T	11.0	...	b; N
MRC B2255−282......	0.98	1733	−0.23	1676	1320	>5	U	<1	...	g
MRC B2256−217......	1.33	64:	1.23:	7	9	0.085	T	33.2	0.45n	b
MRC B2257−270......	1.45	310	0.62	...	160	CSS	U	<1	...	b
MRC B2338−233......	1.00	130:	0.82:	<1	<4	<0.009	D	29.5	0.25n	b
MRC B2338−290......	1.28:	159:	0.75:	53	37	0.65	T	73	1.0	g; N
MRC B2348−252......	4.41	270:	1.13:	6.3	32	0.020	T	33.5	0.3w	b

Column (*9*).—Logarithm of the 408 MHz radio power, P_{408}, measured in W Hz^{-1} ($H_0 = 50$ km s^{-1} Mpc^{-1} and $q_0 = 0.5$ used for both power and linear size).

Column (*10*).—Largest linear size, *l*, in kpc (see under col. [9]).

Column (*11*).—" N " indicates additional notes in § 4.

4. NOTES ON INDIVIDUAL SOURCES

MRC B0022−297.—A faint jet is visible connecting the core to the brightest feature in the northern lobe.

MRC B0030−220.—The core component is not well resolved in the 4.86 GHz image but is clearly seen at 8.44 GHz with $S_{8.44}$(core) = 9.5 mJy and $S_{8.44}$(total) = 46 mJy.

MRC B0106−233.—The southern lobe in the 4.86 GHz image is completely resolved out at 8.44 GHz. The souteast extension to the northern lobe seen in the 8.44 GHz image is probably due to the core ($S^{\rm core}_{8.44} = 5$ mJy). The two lobes would thus appear to be misaligned by about 33° from collinearity with the core.

MRC B0111−256.—With a restoring beam of 9″.5 × 2″.75 (PA 45°), the source appears barely resolved, having a deconvolved size of 2″.2 in PA 161°.

MRC B0118−272.—A known BL Lac object with an absorption-line system at a redshift of 0.557 (Falomo 1991; Stickel, Fried, & Kühr 1993).

MRC B0123−226.—The extended structure is mostly resolved out in the 8.44 GHz image, with $S_{8.44}$(core) = 98 mJy.

MRC B0222−224.—No detected core component in either the 4.86 GHz or 8.44 GHz images. The flux density measured on the PTI baseline is likely to refer to fine structure in the two closely spaced radio lobes.

MRC B0237−233.—A good example of a GPS source, with a convex radio spectrum peaking at ~1 GHz.

MRC B0301−243.—The source has a strong radio core and an extended diffuse halo-like component extending over ~60″. The core coincides with a relatively bright stellar object with a lineless spectrum characteristic of a BL Lac object (see also Véron-Cetty & Véron 1993).

MRC B0338−294.—The brightest parts of the two lobes are misaligned by ~37° from collinearity with the core.

MRC B0338−214.—A flat-spectrum source known to be a BL Lac object (Wright et al. 1977; Falomo, Scarpa, & Bersanelli 1994).

MRC B0338−259.—The source has a relatively strong radio core whose position coincides with a faint stellar

TABLE 4

Optical Identifications for the Molongo Quasar Sample

Source (1)	Radio Position (B1950.0) R.A. (2)	Radio Position (B1950.0) Decl. (3)	Optical Position R.A. (4)	Optical Position Decl. (5)	Optical Position Reference Code (6)	b_J (7)	z (8)	log P_{408} (W Hz^{-1}) (9)	l (kpc) (10)	Notes (11)
MRC B0017−207......	00 17 49.83	−20 45 29.9	49.82	30.3	1	19.3	0.545	27.28	705.9	
MRC B0022−297......	00 22 00.24	−29 45 31.6	00.26	32.5	2	18.8	0.406	27.80	284.9	N
MRC B0029−271......	00 29 21.28	−27 08 58.1	21.31	56.8	1	19.6	0.333	26.82	≤5.8	
MRC B0030−220......	00 30 14.62	−22 00 54.6	14.64	54.1	2	18.9	0.806	27.55	32.1	N
MRC B0040−208......	00 40 29.20	−20 53 39.1	29.18	39.5	3	16.4	0.657	27.40	<15.7	
MRC B0058−229......	00 58 15.53	−22 56 08.6	15.58	09.2	2	21.7	0.706	27.52	503.1	
MRC B0106−233......	01 06 37.59	−23 23 28.8	37.60	29.0	2	20.1	0.818	27.59	20.6	N
MRC B0111−256......	01 11 18.80	−25 39 51.7	18.78	51.4	1	21.1	1.05	27.71	18.8	N
MRC B0118−272......	01 18 09.53	−27 17 07.4	09.45	06.7	3	17.5	>0.557	>27.18	...	N
MRC B0123−226......	01 23 51.27	−22 38 07.6	51.29	07.7	3	19.9	0.717	27.54	40.9	N
MRC B0133−266......	01 33 05.36	−26 38 56.7	05.32	56.3	1	19.9	1.530	28.24	456.3	
MRC B0135−247......	01 35 17.11	−24 46 08.7	17.05	08.6	1	18.9	0.835	27.77	...	
MRC B0136−231......	01 36 35.47	−23 09 59.9	35.50	60.5	3	19.7	1.895	28.29	105.9	
MRC B0142−278......	01 42 44.99	−27 48 35.5	44.96	35.4	1	17.5	1.148	27.63	<8.6	
MRC B0209−237......	02 09 10.47	−23 42 28.4	10.54	29.0	1	19.0	0.680	27.56	142.3	
MRC B0222−234......	02 22 45.99	−23 26 19.6	46.00	19.0	2	18.7	0.230	27.12	72.0	
MRC B0222−224......	02 22 59.05	−22 28 52.4	59.07	52.6	1	19.1	1.617	28.59	20.4	N
MRC B0237−233......	02 37 52.79	−23 22 06.4	52.57	06.2	1	16.4	2.223	28.63	...	N
MRC B0246−231......	02 46 07.99	−23 10 25.9	07.94	25.4	1	21.4	2.904	29.02	<7.4	
MRC B0301−243......	03 01 14.21	−24 18 53.0	14.21	52.7	1	16.4	...	...	...	N
MRC B0315−282......	03 15 26.93	−28 14 15.0	26.92	15.8	5	19.9	1.17	27.76	≤17.2	N
MRC B0327−241......	03 27 43.87	−24 07 22.9	43.88	23.0	1	19.4	0.895	27.53	...	
MRC B0328−272......	03 28 25.97	−27 14 51.5	26.03	51.5	2	18.1	1.803	28.31	151.1	
MRC B0338−294......	03 38 17.30	−29 27 28.0	17.38	28.6	2	18.9	1.139	27.88	90.2	N
MRC B0338−214......	03 38 23.21	−21 29 09.0	23.23	06.8	1	16.0	0.048	25.09	<1.3	N
MRC B0338−259......	03 38 32.40	−25 57 12.0	32.58	12.5	5	22.6r	...	...	...	N
MRC B0346−279......	03 46 34.03	−27 58 20.7	34.09	19.6	1	20.5	0.989	27.56	...	
MRC B0407−226......	04 07 47.84	−22 36 21.2	47.87	22.3	3	21.8r	1.480	28.25	197.6	
MRC B0413−296......	04 13 08.89	−29 36 30.4	08.86	31.0	2	18.4	1.630	28.84	330.4	
MRC B0413−210......	04 13 53.62	−21 03 51.0	53.59	51.1	2	18.6	0.807	28.36	41.2	N
MRC B0418−288......	04 18 35.90	−28 48 20.0	35.93	20.0	1	21.1	0.85	27.67	<16.6	
MRC B0421−225......	04 21 45.57	−22 30 52.4	45.57	52.3	1	17.5	0.364	27.03	49.6	N
MRC B0430−278......	04 30 16.60	−27 52 43.8	16.65	43.2	4	21.3	1.63	28.12	<16.9	
MRC B0437−244......	04 37 03.92	−24 27 59.9	03.93	58.9	3	17.5	0.84	27.69	1045.9	
MRC B0439−299......	04 39 21.91	−29 58 18.5	21.94	17.8	1	20.4	...	...	...	N
MRC B0447−230......	04 47 03.57	−23 04 07.1	03.60	07.1	3	22.0	2.14	28.41	<16.1	
MRC B0450−221......	04 50 36.95	−22 06 14.5	36.93	14.8	2	17.8	0.898	28.21	120.0	
MRC B0451−282......	04 51 15.13	−28 12 29.4	15.20	29.2	3	17.8	2.560	28.49	...	
MRC B0454−220......	04 54 01.14	−22 03 49.5	01.13	50.0	2	18.6	0.533	27.83	612.5	
MRC B0522−215......	05 22 40.74	−21 33 17.4	40.73	17.0	3	22.0	1.83	28.60	20.8	N
MRC B0549−213......	05 49 50.60	−21 20 30.0	50.56	29.6	1	19.1	2.245	28.70	28.7	N
MRC B0925−203......	09 25 33.54	−20 21 45.0	33.50	45.1	3	16.4	0.346	26.80	...	
MRC B0941−200......	09 41 30.22	−20 05 44.5	30.22	45.1	2	17.9	0.715	27.44	382.1	
MRC B1006−299......	10 06 39.70	−29 56 27.5	39.70	28.1	2	18.0	1.064	27.97	156.6	
MRC B1010−271......	10 10 09.73	−27 11 24.2	09.68	24.2	1	18.9	0.436	27.15	296.7	
MRC B1011−282......	10 11 12.33	−28 16 32.0	12.33	31.4	2	16.3	0.255	26.91	318.2	N
MRC B1017−248......	10 17 46.31	−24 49 32.0	...	...	...	≥22.5	...	...	...	N
MRC B1019−227......	10 19 05.73	−22 46 46.4	05.73	45.4	2	21.1	1.55	28.17	18.7	N
MRC B1025−229......	10 25 32.42	−22 56 42.4	32.43	41.5	4	16.7	0.309	26.71	1051.4	N
MRC B1025−264......	10 25 49.14	−26 28 57.3	49.15	57.8	2	17.5	2.665	28.70	77.3	N
MRC B1043−291......	10 43 19.02	−29 11 38.1	18.96	37.1	1	18.6	2.128	28.14	<8.1	
MRC B1052−272......	10 52 52.88	−27 13 50.6	52.86	52.0	3	22.2	1.103	28.20	656.3	
MRC B1055−242......	10 55 29.94	−24 17 44.6	29.95	45.0	1	19.9	1.090	27.99	...	
MRC B1106−227......	11 06 43.35	−22 45 28.8	43.32	28.3	1	20.8	1.875	28.51	<8.3	
MRC B1114−220......	11 14 26.02	−22 02 29.0	26.08	29.4	2	20.2	2.282	28.63	<7.9	
MRC B1117−248......	11 17 40.92	−24 51 41.4	40.96	41.9	1	17.3	0.462	27.40	...	
MRC B1121−238......	11 21 34.89	−23 48 51.0	34.95	51.1	1	18.6	0.675	27.61	362.8	
MRC B1151−298......	11 51 16.80	−29 53 04.8	16.80	05.1	1	18.1	1.376	28.18	34.4	N
MRC B1156−221......	11 56 37.79	−22 11 54.9	37.69	54.9	3	18.6	0.563	27.58	...	
MRC B1202−262......	12 02 58.87	−26 17 22.5	58.85	22.2	2	19.8	0.786	27.97	122.9	N
MRC B1208−277......	12 08 08.54	−27 42 18.0	08.57	17.9	2	18.8	0.828	27.74	359.3	
MRC B1212−275......	12 12 26.94	−27 33 32.0	26.98	31.3	2	19.6	1.656	28.22	29.6	N
MRC B1217−209......	12 17 46.10	−20 56 36.7	46.06	36.8	4	20.2	0.814	27.56	245.9	
MRC B1222−293......	12 22 23.68	−29 21 42.9	23.68	43.4	2	18.5	0.816	27.64	242.7	N
MRC B1224−262......	12 24 02.74	−26 13 26.0	02.76	25.3	1	19.8	0.768	27.98	<16.3	
MRC B1226−297......	12 26 06.19	−29 46 03.4	06.18	03.5	2	17.0	0.749	27.54	522.7	
MRC B1232−249......	12 32 59.35	−24 55 45.7	59.36	45.8	2	17.0	0.352	27.47	655.9	
MRC B1244−255......	12 44 06.71	−25 31 26.7	06.64	26.9	1	16.2	0.635	27.24	...	
MRC B1247−290......	12 47 28.40	−29 00 15.2	28.45	14.2	4	22.1	0.770	27.77	469.7	

TABLE 4—*Continued*

Source (1)	Radio Position (B1950.0) R.A. (2)	Decl. (3)	Optical Position R.A. (4)	Decl. (5)	Reference Code (6)	b_J (7)	z (8)	log P_{408} (W Hz^{-1}) (9)	l (kpc) (10)	Notes (11)
MRC B1256−220......	12 56 13.94	−22 03 20.4	13.89	20.6	1	19.6	1.303	27.73	...	
MRC B1256−243......	12 56 31.27	−24 19 55.2	31.25	55.2	2	17.6	2.263	28.24	65.2	N
MRC B1257−230......	12 57 43.91	−23 01 56.3	44.04	55.7	3	17.1	1.109	28.40	446.3	
MRC B1301−251......	13 01 32.30	−25 08 31.5	32.30	32.2	2	21.0	0.952	27.73	73.6	
MRC B1302−208......	13 02 18.38	−20 50 38.7	18.30	38.7	3	21.8	...	...	...	N
MRC B1303−250......	13 03 32.86	−25 01 17.6	32.86	18.2	2	17.7	0.738	27.61	310.9	N
MRC B1309−216......	13 09 49.62	−21 40 29.2	49.61	29.3	1	18.5	>1.49	>28.05	25.6	N
MRC B1311−270......	13 11 02.94	−27 00 56.5	02.92	56.6	2	19.3	2.186	28.69	156.4	N
MRC B1327−214......	13 27 23.38	−21 26 33.8	23.36	33.8	2	16.4	0.528	27.88	225.2	
MRC B1348−289......	13 48 55.86	−28 57 29.1	55.84	29.6	1	19.3	...	...	...	N
MRC B1349−265......	13 49 20.94	−26 34 40.6	20.96	40.8	1	18.4	0.934	28.15	<16.9	
MRC B1351−211......	13 51 25.43	−21 08 28.9	25.41	28.9	1	18.2	1.262	28.33	94.7	N
MRC B1355−236......	13 55 44.58	−23 37 47.2	44.60	47.3	2	17.8	0.832	27.74	132.6	
MRC B1355−215......	13 55 51.46	−21 34 21.4	51.49	21.7	1	19.9	1.604	28.42	35.6	N
MRC B1359−281......	13 59 10.61	−28 07 58.7	10.56	59.0	1	18.7	0.802	27.80	11.5	N
MRC B2021−208......	20 21 38.58	−20 53 37.4	38.55	38.1	2	18.3	1.2	28.22	210.9	
MRC B2024−217......	20 24 09.21	−21 46 13.8	09.20	14.0	1	19.1	0.459	27.40	212.5	
MRC B2025−206......	20 25 15.24	−20 38 37.1	15.28	37.0	3	18.7	1.40	28.43	279.0	
MRC B2030−230......	20 30 20.48	−23 03 33.5	20.51	33.5	1	19.1	0.132	26.71	216.0	
MRC B2035−203......	20 35 34.90	−20 21 42.0	34.88	42.8	2	16.4	0.516	27.37	460.8	N
MRC B2037−234......	20 37 12.71	−23 27 08.7	12.70	08.7	3	22.4	1.15	27.86	128.9	N
MRC B2040−236......	20 40 13.94	−23 37 37.7	13.95	37.4	3	16.8	0.704	27.37	446.8	
MRC B2059−214......	20 59 08.95	−21 25 48.1	09.00	49.1	5	23.1r	...	...	...	N
MRC B2111−259......	21 11 44.79	−25 54 19.4	44.79	19.5	4	18.1	0.602	27.99	68.5	N
MRC B2122−238......	21 22 59.88	−23 51 11.9	59.89	11.7	1	17.8	1.774	28.22	13.4	N
MRC B2128−208......	21 28 12.27	−20 50 09.7	12.22	10.0	4	20.0	1.620	29.01	<17.0	
MRC B2136−251......	21 36 21.32	−25 07 50.5	21.32	51.2	3	18.1	0.940	27.67	<16.9	N
MRC B2149−200......	21 49 04.35	−20 00 10.8	04.39	12.1	3	17.8	0.424	27.66	13.2	N
MRC B2156−245......	21 56 35.76	−24 32 16.0	35.78	16.8	2	20.2	0.862	27.74	<16.7	
MRC B2158−206......	21 58 40.80	−20 40 03.4	40.80	03.8	2	20.1	2.272	28.56	<7.9	
MRC B2210−257......	22 10 14.13	−25 44 22.4	14.00	23.6	3	17.9	1.831	28.19	...	
MRC B2211−251......	22 11 16.45	−25 11 38.2	16.43	38.3	1	19.6	2.508	29.01	18.5	N
MRC B2213−283......	22 13 10.31	−28 18 28.5	10.33	29.2	2	16.5	0.946	28.12	490.5	
MRC B2227−214......	22 27 53.88	−21 28 19.5	53.88	19.0	2	19.6	1.410	28.36	129.6	
MRC B2232−272......	22 32 23.22	−27 16 21.5	23.23	21.5	2	19.5	1.495	28.16	136.8	N
MRC B2240−260......	22 40 41.83	−26 00 15.8	41.86	16.3	2	17.9	0.774	27.51	89.8	N
MRC B2255−282......	22 55 22.41	−28 14 26.0	22.48	25.8	2	16.6	0.927	27.34	<8.4	
MRC B2256−217......	22 56 34.37	−21 43 43.1	34.38	43.4	2	19.9	1.779	28.55	277.8	
MRC B2257−270......	22 57 42.82	−27 00 29.7	42.81	31.0	3	18.3	1.476	28.16	<8.6	
MRC B2338−233......	23 38 09.14	−23 19 19.7	09.09	18.2	2	17.3	0.715	27.41	236.3	
MRC B2338−290......	23 38 13.93	−29 05 19.0	13.96	20.5	2	18.2	0.446	27.08	494.1	N
MRC B2348−252......	23 48 14.61	−25 13 45.4	14.54	45.4	4	17.3	1.386	28.78	287.7	

Note.—In cols. (4) and (5), units of right ascension are seconds, and units of declination are arcseconds.

object seen in our r-band CCD image taken with the 2.5 m du Pont telescope (Fig. 5). This makes it very likely a quasar, although spectroscopic confirmation is required.

MRC B0413−210.—The core component is seen clearly only at 8.44 GHz with a flux density of 525 mJy; at 4.86 GHz, the peak flux density is 510 mJy $beam^{-1}$, and the peak position coincides with the optical. $S_{8.44}$(total) is 935 mJy. The lobes are misaligned by $\sim 50°$ from collinearity with the core.

MRC B0421−225.—The source extension is along PA 56°.

MRC B0439−299.—Probable BL Lac object.

MRC B0522−215.—The source extension is along PA 150°.

MRC B0549−213.—The source appears to have a D2-type structure, with the stronger component ($S_{4.86}$ = 209 mJy) coincident with the optical position of the quasar. The core position listed in Table 4 is for this component. The core would thus appear to have a steep spectrum as the southern component is rather weak ($S_{4.86} \sim 9$ mJy), and the overall spectral index is $\alpha_{0.408}^{4.86} \sim 0.83$.

MRC B1011−282.—This source has a peculiar morphology in our 4.86 GHz image, with the southern compact component coinciding with the optical position of the quasar and a diffuse bridge connecting it to the northern lobe. Previous imaging at 6 and 20 cm by Gower & Hutchings (1984) finds the southern component to have a flat spectrum ($\alpha = 0.26$) between these frequencies. They also report a faint southern lobe about 54″ southeast of the flat-spectrum core. This component is barely seen in our VLA image, with $S_{4.86} \sim 2$ mJy. This extended southern lobe is very clearly seen, however, in recent unpublished images at coarser resolution made with the Australia Telescope compact array at 20 and 13 cm by A. D. Reid and R. W. Hunstead, thus giving the source an overall LAS of $\sim 70''$ and a bent structure with a bend angle of 21°.

MRC B1017−248.—The weak radio core in this source lies within $\sim 2''$ of a faint stellar object visible on the CCD image. The presence of a core and large misalignment ($\sim 38°$) of the lobe hot spots from collinearity with the radio core is strongly suggestive of the source being a quasar. Spectroscopic confirmation was, however, not possible as

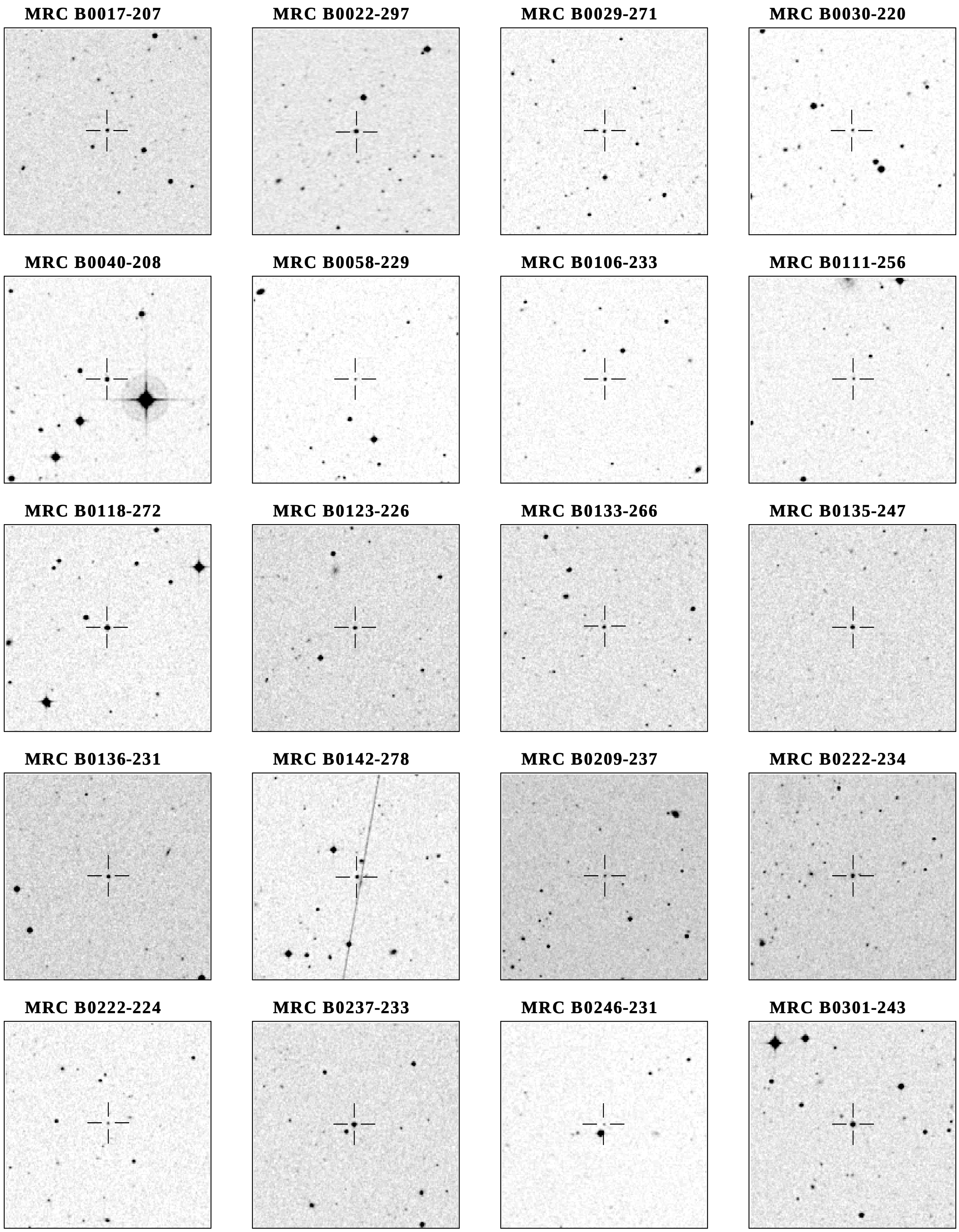

FIG. 4.—Finding charts for the MQS reproduced from the NASA/STScI digitized UK Schmidt III-aJ sky survey. Each field covers a region of 5′ × 5′. North is at the top, and east to the left.

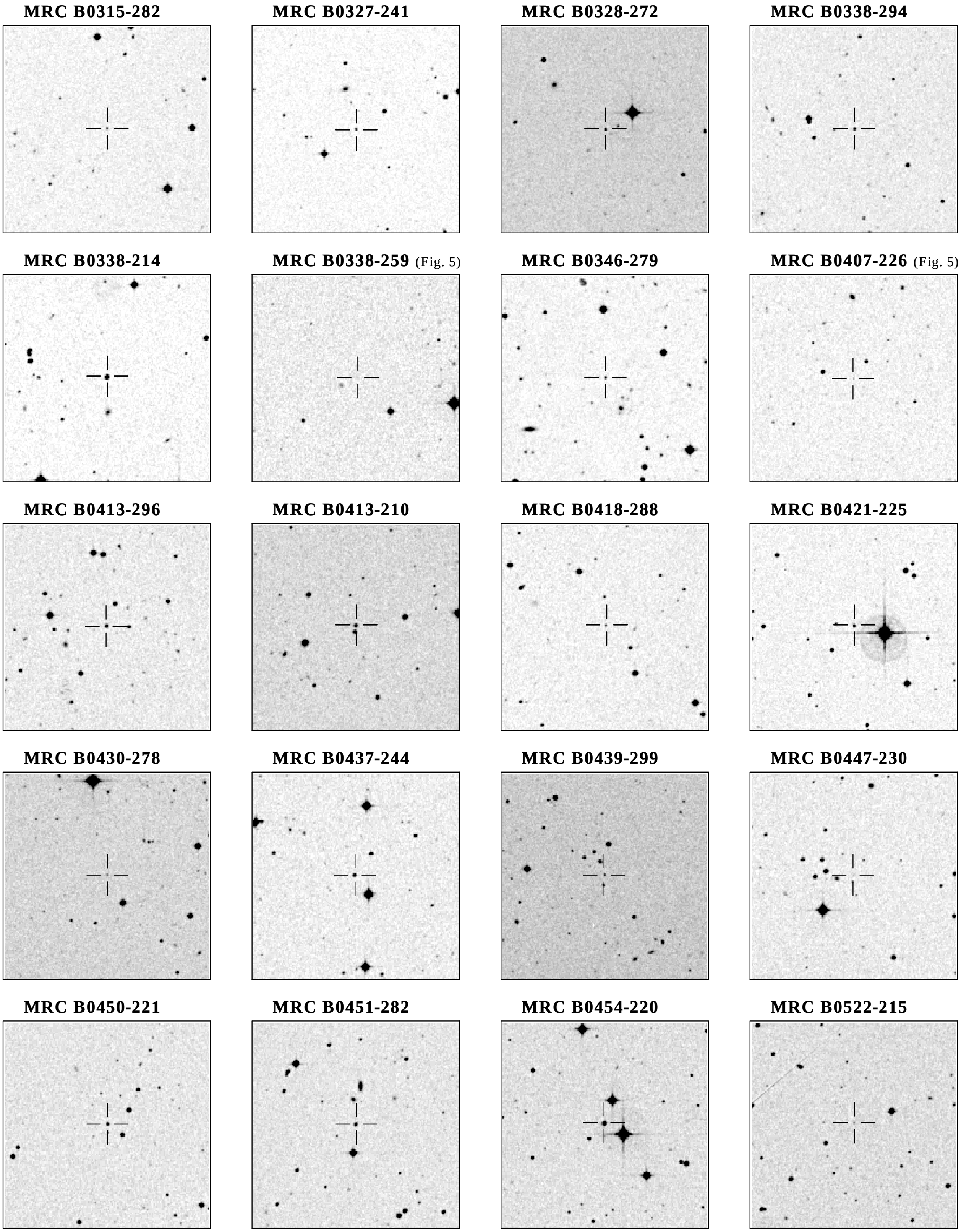

FIG. 4.—*Continued*

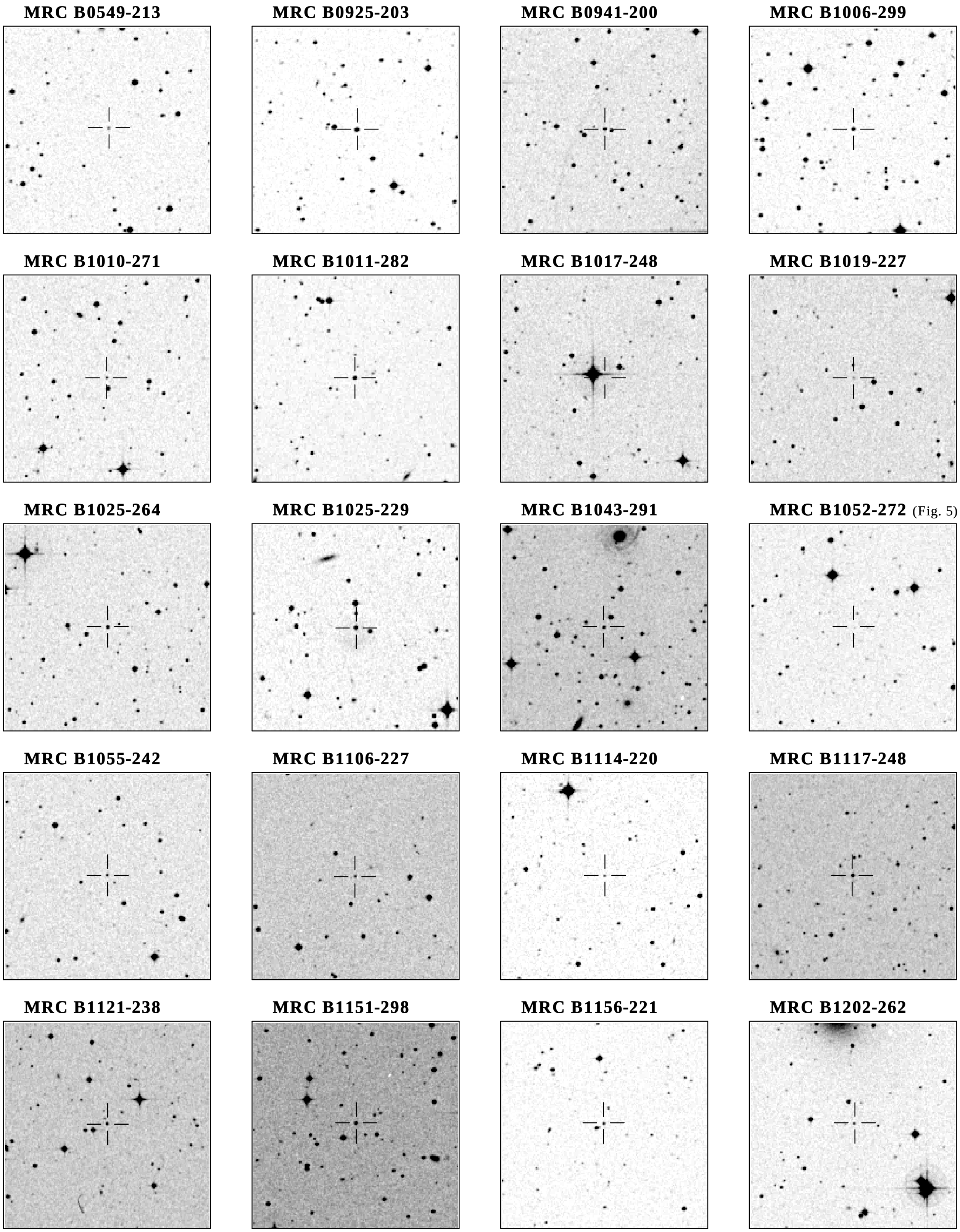

FIG. 4.—*Continued*

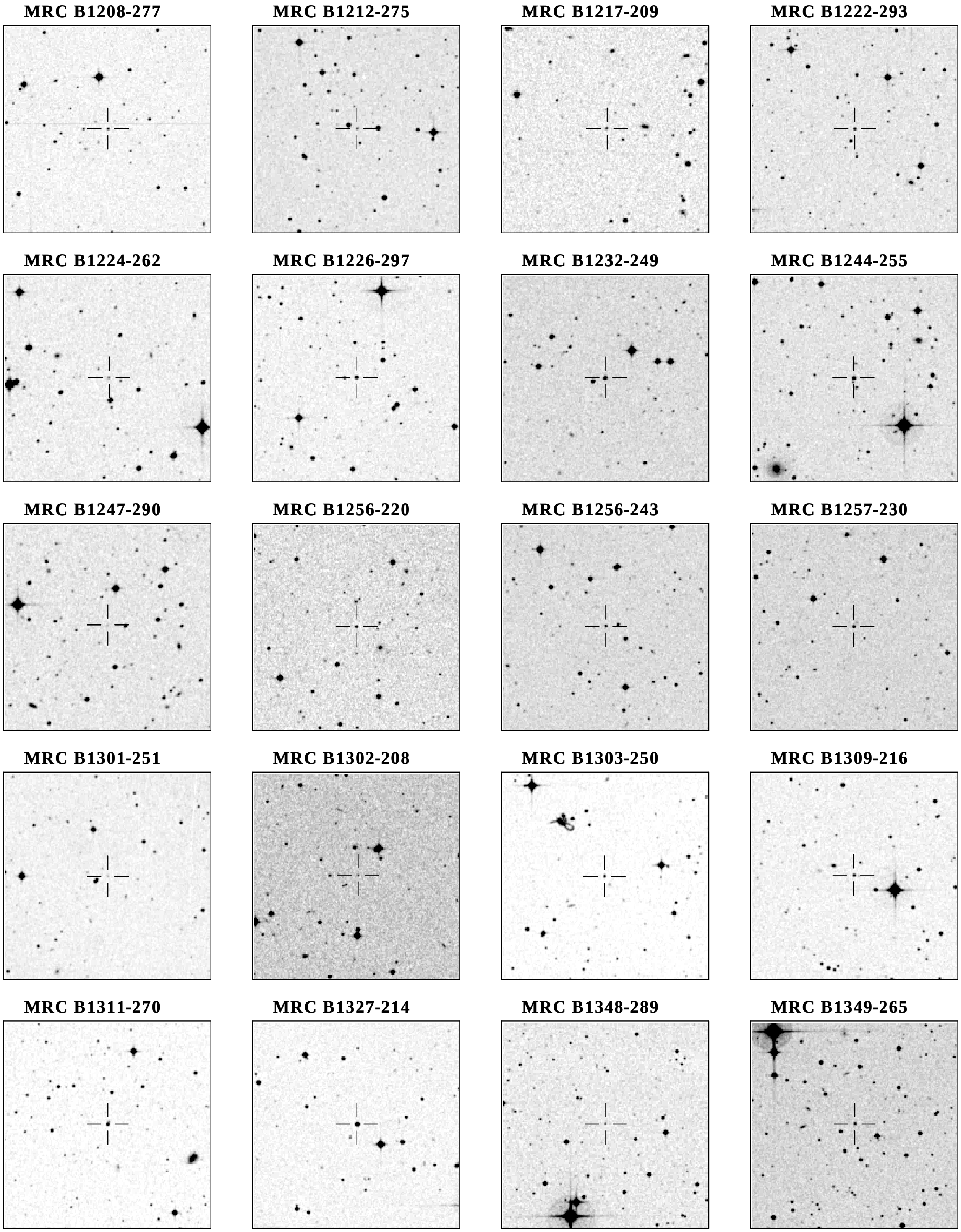

FIG. 4.—*Continued*

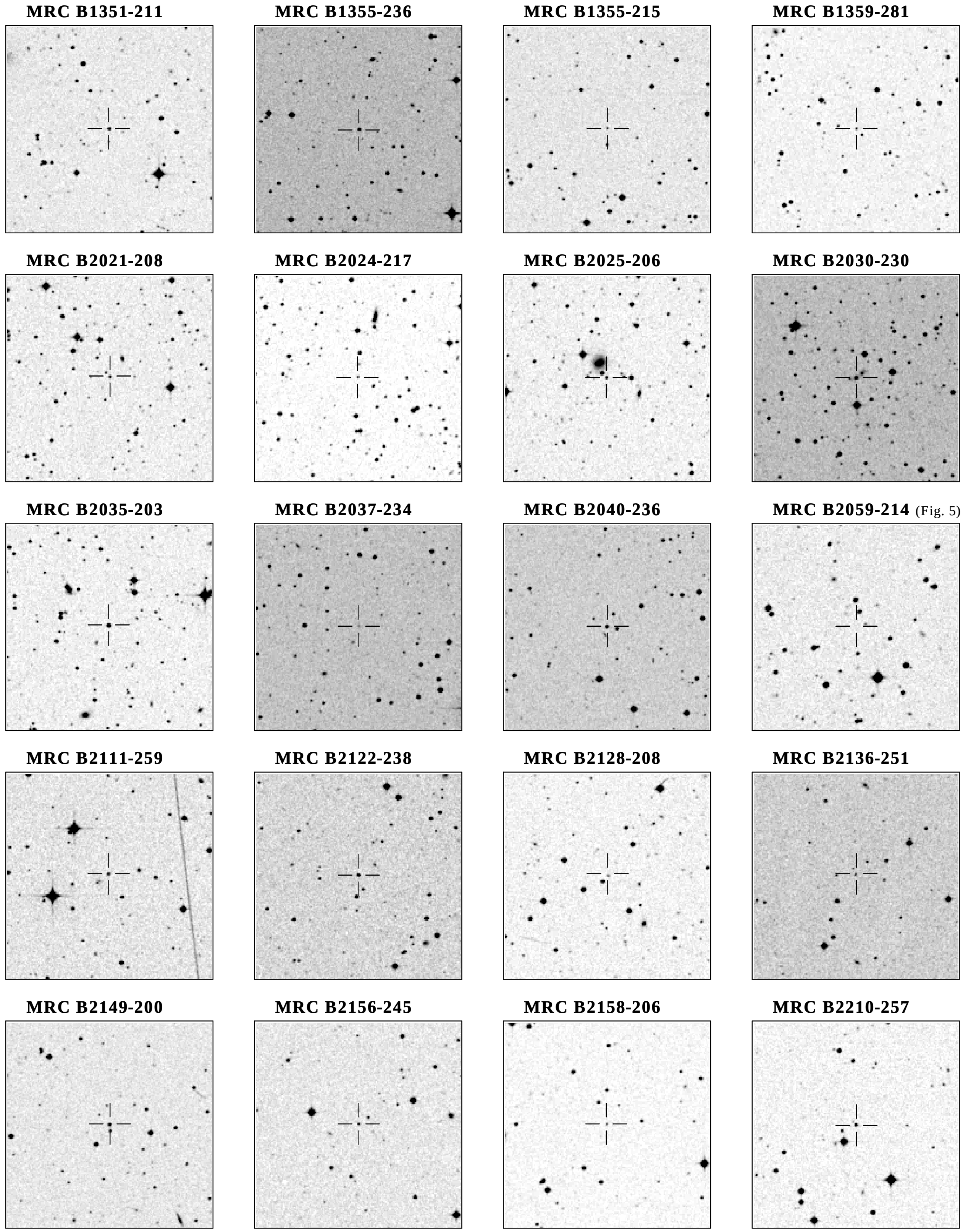

FIG. 4.—*Continued*

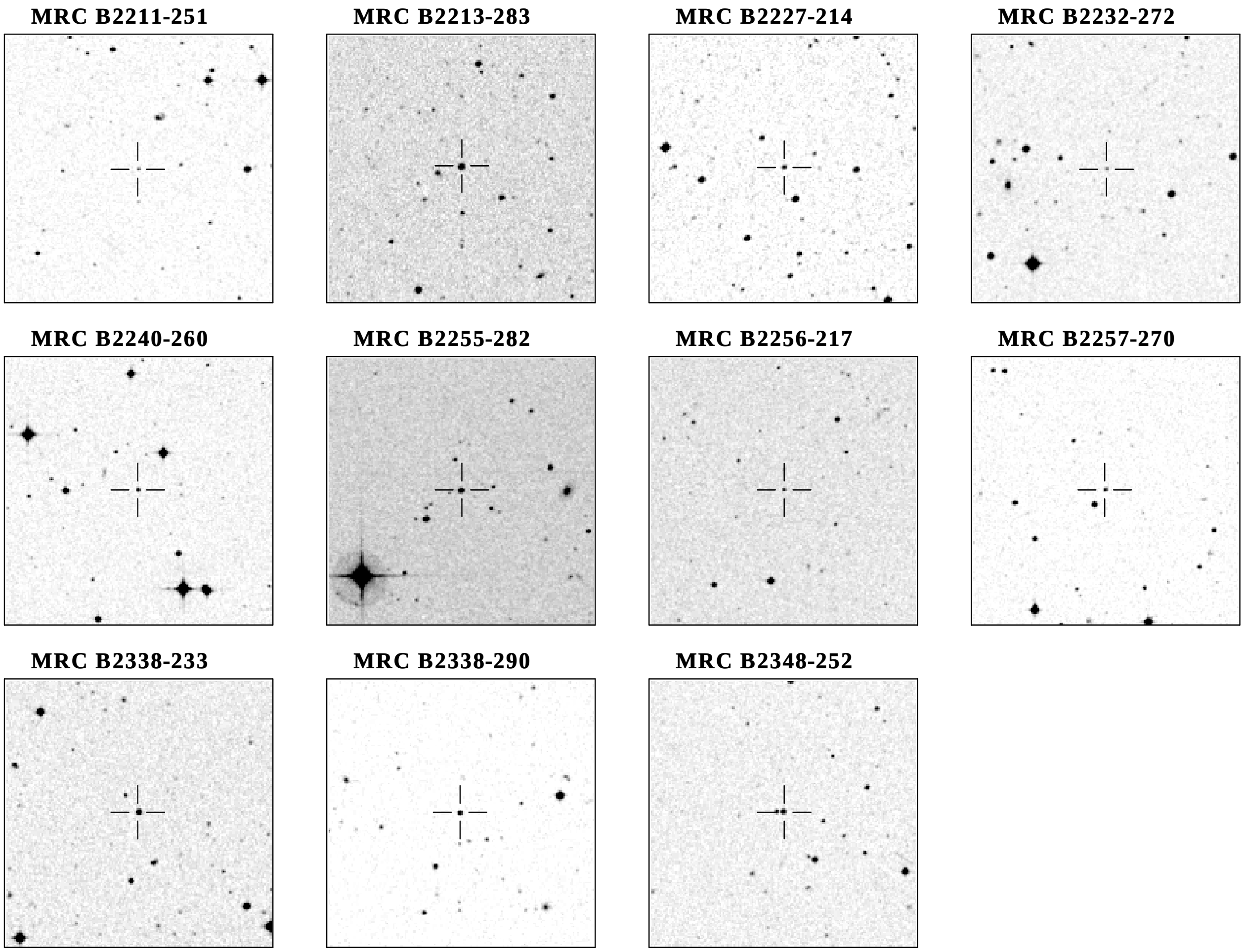

FIG. 4.—*Continued*

the faint optical identification is quite close to a bright star (see finding chart in Fig. 5).

MRC B1019−227.—No obvious core in this close double with LAS = 2".2 along PA 21°; higher resolution is needed.

MRC B1025−229.—Much of the extended structure is resolved out in the 4.86 GHz image of this large quasar; only the hot spots in the two lobes and two compact components near the quasar are visible. The more southerly of the two central components is the radio core, while the other is possibly a knot in a jet toward the northern lobe. The total flux density measured from the 1.41 GHz VLA image (see Fig. 2) is 594 mJy. Because of its large size, the MRC flux density of $S_{408} = 1.05$ Jy is also likely to be an underestimate.

MRC B1025−264.—The source appears to have a D2-type morphology with the strong and compact northwesterly component coincident with the optical position. The overall spectrum of the source is, however, steep, and the core component would thus appear to be also steep spectrum as is evident from the higher flux density measured with PTI at 2.29 GHz.

MRC B1151−298.—The higher resolution 8.44 GHz image (see Fig. 2) shows a core with $S_{8.44} = 2.5$ mJy, about

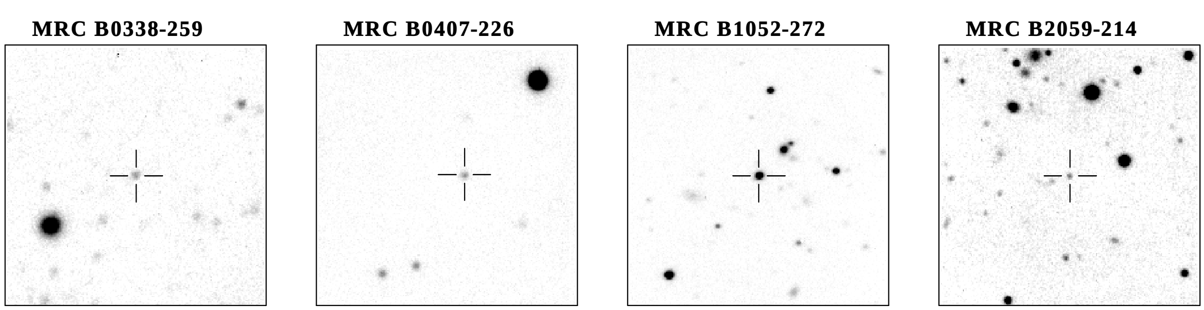

FIG. 5.—Finding charts for four faint quasars reproduced from *r*-band CCD images made with the 2.5 m du Pont telescope at Las Campanas. Each field covers a region of about 66" × 66". North is to the top, and east to the left.

1″ southwest of the northern lobe. The PTI flux of 41 mJy at 2.29 GHz is likely to arise mainly from the hot spot in the northern lobe.

MRC B1202−262.—An unpublished image made from VLA calibration data at 5 GHz (R. Perley, private communication) shows a strong core; the two lobes appear to be misaligned by ∼50° from collinearity with the core.

MRC B1212−275.—The source is extended along PA 61°; there is insufficient resolution to identify the core component.

MRC B1222−293.—The peaks in the two lobes appear to be misaligned from collinearity with the radio core by ∼34°.

MRC B1256−243.—The component ∼2″ south of the core is barely resolved in the 4.86 GHz image but is clearly resolved at 8.44 GHz (Fig. 2). The weak western lobe is resolved out at 8.44 GHz. The lobes are thus misaligned by ∼53° from collinearity with the core.

MRC B1302−208.—The source has possible structure extending ∼4″ north of the strong compact component which is identified with a faint stellar object. Spectroscopy is required to confirm this as a quasar.

MRC B1303−250.—Most of the extended emission in the northwest lobe arises in a long bent jet. The peaks in the two lobes are misaligned by ∼34° from collinearity with the core.

MRC B1309−216.—This is a known BL Lac type object with an absorption redshift 1.489 (Blades, Murdoch, & Hunstead 1980).

MRC B1311−270.—A jetlike feature connects the core to the westerly lobe.

MRC B1348−289.—Identified with a stellar object; needs spectroscopic confirmation.

MRC B1351−211.—Strongly bent structure. The two lobes are misaligned by ∼61° from collinearity with the core.

MRC B1355−215.—The strong central component shows considerable structure in the higher resolution image at 8.44 GHz (Fig. 2). The peak in the brightness distribution (44 mJy beam^{-1}) is likely to be caused by the core component. The western lobe is resolved out at 8.44 GHz.

MRC B1359−281.—The source is slightly extended along PA 116°.

MRC B2035−203.—The 2.29 GHz flux density measured on the PTI baseline is much smaller than the VLA core flux density at 4.86 GHz. It is possible that much of the VLA flux arises from a knot in a jet close to the core.

MRC B2059−214.—The source extension is along PA 131°. The identification with a faint stellar object needs spectroscopic confirmation.

MRC B2111−259.—Highly bent structure, with a bend angle of ∼47°. The higher resolution image at 8.44 GHz shows $S_{8.44}$(core) ∼93 mJy; there is a jet pointing toward the north lobe.

MRC B2122−238.—The source has a D2-type structure with the northern component coincident with the optical position. The higher resolution 8.44 GHz image shows that the northern component is unresolved (<0″.3) and has a flat spectral index $\alpha_{4.86}^{8.44} \sim 0.38$.

MRC B2136−251.—The source was also imaged at 1.41 GHz where it is unresolved with a restoring beam of 15″.3 × 9″.3, PA 50°; $S_{1.41}$(total) is 538 mJy.

MRC B2149−200.—D2-type structure. The higher resolution 8.44 GHz image shows that the northern component is likely to be the core as it has a flat spectrum with $\alpha_{4.86}^{8.44} \sim 0.17$. The stronger southern component has $\alpha_{4.86}^{8.44} \sim 0.79$. Part of the flux recorded by PTI could be from the southern lobe.

MRC B2211−251.—The source appears to have a D2-type structure with the stronger northwest component ($S_{4.86} \sim 170$ mJy) coincident with the quasar. If this component is indeed the radio core, it must have a steep spectrum as the overall spectral index of the source is $\alpha_{0.408}^{4.86} \sim 0.98$.

MRC B2232−272.—The 8.44 GHz image confirms that the western component consists of a long jet (with two sharp bends in it) without any extended lobe emission.

MRC B2240−260.—This is a known BL Lac object at $z = 0.774$ (Stickel et al. 1993); there is weak diffuse emission around a strong radio core.

MRC B2338−290.—The source has a bent structure with a bend angle of ∼33°. There is a nearby source (almost definitely unrelated) at R.A. = 23^{h}38^{m}05^s.00, decl. = −20°05′13″ (1950.0) with $S_{4.86} \sim 69$ mJy.

5. OPTICAL FINDING CHARTS

For the sake of completeness and ease of reference we have extracted the finding charts for all 111 objects in the sample from the NASA/STScI digitized UK Schmidt III-aJ sky survey (Morrison 1995), and these are presented in Figure 4. Each field covers a region of 5′ × 5′ and is centered on the optical position of the quasar. In the case of four objects that are too faint to be recorded by the Schmidt survey, finding charts have been prepared from our *r*-band CCD images made with the 2.5 m du Pont telescope of the Las Campanas Observatory. These images cover a region of 66″ × 66″ and are presented in Figure 5.

6. SUMMARY

We have defined a new complete sample of radio quasars, the Molonglo Quasar Sample, selected from the MRC with $S_{408} \geq 0.95$ Jy. The MQS contains 105 quasars, of which 100 have been confirmed spectroscopically, and six BL Lac objects. Only 32 of the quasars were known previously. Basic radio and optical data have been presented in this paper, including VLA radio images of extended sources and a complete set of optical finding charts.

An important feature of the MQS is its significantly higher completeness level compared with most existing quasar samples. This is because it has been defined on the basis of practically complete optical identifications of a large flux-limited sample of radio sources and subsequent spectroscopy of likely quasar candidates. The optical counterparts of four quasars in the sample are in fact too faint to be visible on the deep UK Schmidt sky survey plates with a limiting magnitude of $b_J \sim 22.5$. The spectroscopic observations of a good fraction of the faint plate-limit objects have also been invaluable in deciding the quasar or galaxy nature of the identifications. The overall completeness level of our quasar sample is estimated to be greater than 95%.

It is this high level of completeness, together with the low selection frequency, that ensures that the MQS does not suffer from orientation-dependent biases. The 3CRR is the only other sample that is similarly unbiased. This property means that the MQS is suited ideally for studies of anisotropic effects in quasars.

The Very Large Array is part of the National Radio Astronomy Observatory, which is operated by Associated Universities Inc., under contract with the National Science Foundation. MOST is operated by the University of Sydney with support from the Australian Research Council. J. C. B. was supported from 1992 to 1994 by a graduate scholarship from the Special Research Centre for Theoretical Astrophysics at the University of Sydney. The work by W. vB. at IGPP/LLNL was performed under the auspices of the US Department of Energy under contract W-7405-ENG-48.

REFERENCES

Antonucci, R. R. J. 1993, ARA&A, 31, 473
Baars, J. W. M., Genzel, R., Pauliny-Toth, I. I. K., & Witzel, A. 1977, A&A, 61, 99
Baker, J. C. 1994, Ph.D. thesis, Univ. of Sydney
———. 1997, MNRAS, 286, 23
Baker, J. C., & Hunstead, R. W. 1995, ApJ, 452, L95
Baker, J. C., Hunstead, R. W., Kapahi, V. K., & Subrahmanya, C. R. 1998, ApJS, in press (Paper IV)
Blades, J. C., Murdoch, H. S., & Hunstead, R. W. 1980, MNRAS, 191, 61
Browne, I. W. A., & Wright, A. E. 1985, MNRAS, 213, 97
Drinkwater, M. J., Barnes, D. G., & Ellison, S. L. 1995, Proc. Astron. Soc. Australia, 12, 248
Ekers, R. D., et al. 1989, MNRAS, 236, 737
Fanti, C., Fanti, R., Formiggini, L., Lari, C., & Padrielli, L. 1977, A&AS, 28, 351
Falomo, R. 1991, AJ, 102, 1991
Falomo, R., Scarpa, R., & Bersanelli, M. 1994, ApJS, 93, 125
Gower, A. C., & Hutchings, J. B. 1984, AJ, 89, 1658
Griffith, M. R., Wright, A. E., Burke, B. F. & Ekers, R. D. 1994, ApJS, 90, 170
Hooley, A., Longair, M. S., & Riley, J. M. 1978, MNRAS, 182, 127
Hunstead, R. W. 1991, Australian J. Phys., 44, 743
———W. 1994, Australian J. Phys., 47, 657
Jackson, N., & Browne, I. W. A. 1989, Nature, 338, 485
Kapahi, V. K., Athreya, R. M., Subrahmanya, C. R., Hunstead, R. W., Baker, J. C., McCarthy, P. J., & van Breugel, W. 1995, J. Astrophys. Astron. Suppl., 16, 125
Kapahi, V. K., Athreya, R. M., Subrahmanya, C. R., McCarthy, P. J., & van Breugel, W. 1998, ApJS, 118, 275 (Paper II)
Kapahi, V. K., & Saikia, D. J. 1982, J. Astrophys. Astron., 3, 465
Kapahi, V. K., & Shastri, P. 1987, MNRAS, 224, 17P
Laing, R. A., Riley, J. M., & Longair, M. S. 1983, MNRAS, 204, 151
Large, M. I., Mills, B. Y., Little, A. G., Crawford, D. F., & Sutton, J. M. 1981, MNRAS, 194, 693
McCarthy, P. J., Kapahi, V. K., van Breugel, W., Persson, S. E., Athreya, R. M., & Subrahmanya, C. R. 1996, ApJS, 107, 19 (Paper I)
McCarthy, P. J., Kapahi, V. K., van Breugel, W., & Subrahmanya, C. R. 1990, AJ, 100, 1014
McCarthy, P. J., van Breugel, W., Kapahi, V. K., & Subrahmanya, C. R. 1991, AJ, 102, 522
Morrison, J. E. 1995, in ASP Conf. Proc. 77, Astronomical Data Analysis Software and Systems IV, ed. R. A. Shaw, H. E. Payne, & J. J. E. Haynes (San Francisco: ASP), 179
Norris, R. P. 1989, User Guide to PTI Data Reduction, ATNF, CSIRO, Australia
Norris, R. P., Kesteven, M. J., Wellington, K. J., & Batty, M. J. 1988, ApJS, 67, 85
Orr, M. J. L., & Browne, I. W. A. 1982, MNRAS, 200, 1067
Perley, R. A. 1982, AJ, 87, 859
Robertson, J. G. 1991, Australian J. Phys., 44, 729
Stannard, D., & Neal, D. S. 1977, MNRAS, 179, 719
Stickel, M., Fried, J. W., & Kühr, H. 1993, A&AS, 98, 393
Subrahmanya, C. R., & Hunstead, R. W. 1986, A&A, 170, 27
Véron-Cetty, M.-P., & Véron, P. 1993, A&AS, 100, 521
Vigotti, M., Vettolani, G., Merighi, R., Lahulla, J. F., & Pedani, M. 1997, A&AS, 123, 219
Wills, D. 1979, ApJS, 39, 291
Wills, D., & Lynds, R. 1978, ApJS, 36, 317
Wright, A. E., Jauncey, D. L., Peterson, B. A., & Condon, J. J. 1977, ApJ, 211, L115
Yentis, D. J., et al. 1992, in Digitised Optical Sky Surveys, ed. H. T. MacGillivray & E. B. Thomson (Dordrecht: Kluwer), 67